Accepted Manuscript

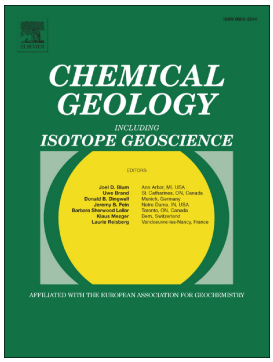

The origin of hydrothermal chlorite- and anhydrite-rich sediments in the middle Okinawa Trough, East China Sea

Hebin Shao, Shouye Yang, Susan Humphris, Di Cai, Feng Cai, Jiangtao Li, Qing Li

PII: S0009-2541(17)30307-8
DOI: doi: 10.1016/j.chemgeo.2017.05.020
Reference: CHEMGE 18351

To appear in: *Chemical Geology*

Received date: 11 December 2016
Revised date: 7 May 2017
Accepted date: 18 May 2017

Please cite this article as: Hebin Shao, Shouye Yang, Susan Humphris, Di Cai, Feng Cai, Jiangtao Li, Qing Li , The origin of hydrothermal chlorite- and anhydrite-rich sediments in the middle Okinawa Trough, East China Sea, *Chemical Geology* (2017), doi: 10.1016/j.chemgeo.2017.05.020

The origin of hydrothermal chlorite- and anhydrite-rich sediments in the middle Okinawa Trough, East China Sea

Hebin Shao [a,b], Shouye Yang [a,b*], Susan Humphris [c*], Di Cai [a], Feng Cai [d], Jiangtao Li [a], Qing Li [d]

a State Key Laboratory of Marine Geology, Tongji University, Shanghai 20092, China

b Laboratory for Marine Geology, Qingdao National Laboratory for Marine Science and Technology, Qingdao 266061, China

c Departments of Geology and Geophysics, Woods Hole Oceanographic Institution, Woods Hole, MA 02543, USA

d Key Laboratory of Marine Hydrocarbon Resources and Environmental Geology, Ministry of Land and Resources, Qingdao Institute of Marine Geology, Qingdao 266071, China

* Corresponding authors:

Dr Shouye Yang

E-mail: syyang@tongji.edu.cn

Dr. Susan Humphris

E-mail: shumphris@whoi.edu

Abstract

During the Integrated Ocean Drilling Program (IODP) Expedition 331, five sites were drilled into the Iheya North Knoll hydrothermal system in the Okinawa Trough (OT) — a back-arc basin characterized by thick terrigenous sediment. Following up on the previous study by Shao et al. (2015), we present new mineralogical, geochemical, and Sr-Nd isotope data to investigate the origin of the hydrothermal sediments and characterize the hydrothermal system. The substrate at the Iheya North Knoll is dominated by pumiceous sediment and other volcanoclastic materials interbedded with hemipelagic (terrigenous and biogenous) sediments. Impermeable layers separate the hydrothermal sediments into distinct units with depth that are characterized by various assemblages of alteration materials, including polymetallic sulfides, sulfates, chlorite- and kaolinite-rich sediments. The rare earth elements (REEs) and Nd isotope data suggest that the chlorite-rich and kaolinite-rich layers primarily resulted from the alteration of pumiceous materials in different chemical and physical conditions. Kaolinite-rich sediment likely reflects low pH and low Mg concentration fluids, while chlorite-rich sediment formed from fluids with high pH and increased Mg contents, likely at higher temperatures. The Sr isotopic compositions of subsurface anhydrite reflect high seawater/hydrothermal fluid ratios in the mid-OT hydrothermal area. Compared with chlorite-rich sediments from other sediment-covered or felsic-hosted hydrothermal systems, the chlorite-rich sediments in the mid-OT are characterized by lower concentrations of Al and Fe but much higher Y, Zr, Hf, Th and REEs, indicative of the distinct nature of the precursor rocks in this region.

Key words: Hydrothermal alteration, chlorite-rich sediments, Okinawa Trough, terrigenous, pumice, Sr-Nd isotopes, Integrated Ocean Drilling Program

1. Introduction

Hydrothermal systems primarily occur in three different spreading environments: mid-ocean ridges, intraoceanic back-arc rifts in ocean crust (such as the Manus Basin, N. Fiji Basin and Lau Basin), and intracontinental rifts in continental crust (such as the Okinawa Trough, East China Sea) (Herzig and Hannington, 1995; Herzig and Hannington, 2000; Glasby and Notsu, 2003). The hydrothermal fields in the Okinawa Trough (OT) are characterized by a thick covering of terrigenous sediments that play an important role in determining the nature of hydrothermal deposits (Lee et al., 1980; Letouzey and Kimura, 1986; Kawagucci et al., 2011). In addition, volcanic materials like pumice are widely distributed in the OT and also affect the geochemistry of hydrothermal alteration reactions (Shinjo, 1999; Shinjo et al., 1999; Shinjo and Kato, 2000; Expedition 331 Scientists, 2011).

Hydrothermal alteration of rocks and sediments results in the formation of secondary mineral assemblages of kaolinite, illite, smectite, montmorillonite, chlorite and other mixed layer clays (Alt, 1999; Marumo and Hattori, 1999; Lackschewitz et al., 2000b; Lackschewitz et al., 2004; Dekov et al., 2005; Miyoshi et al., 2013; Beaufort et al., 2015). The Iheya North Knoll hydrothermal field in the mid-OT is characterized by high concentrations of chlorite, reaching up to 70% at Integrated Ocean Drilling Program (IODP) Site C0013 (Expedition 331 Scientists, 2011). Shao et al. (2015) compared the mineralogy and geochemistry of the clay-size sediments in the mid-OT recovered during the IODP Expedition 331, and discriminated the clay origins between hydrothermal and terrigenous sources. However, whether the chlorite-rich sediments result from hydrothermal alteration of terrigenous sediments and/or volcanic materials remains to be

clarified.

Anhydrite, which exhibits retrograde solubility, is the most important sulfate phase at the mid-OT hydrothermal area (Expedition 331 Scientists, 2011). The precipitation of anhydrite provides the opportunity to investigate the extent of seawater entrainment into the subsurface (Mills and Elderfield, 1995; Humphris, 1998; Teagle et al., 1998a; Teagle et al., 1998b). However, little is known about subsurface circulation within the mid-OT hydrothermal area, where substantial amounts of anhydrite were found during IODP 331 Expedition

To better understand the hydrothermal environment and deposits in the mid-OT area, we have analyzed the bulk mineralogical, elemental and Sr-Nd isotopic compositions of selected samples from several sediment cores collected during IODP Expedition 331. The main objectives of this study are to: 1) determine the nature of the material hydrothermally altered to produce the chlorite-rich sediment in the mid-OT; 2) use the behavior of Sr and the REEs in anhydrite to establish the role of seawater entrainment and subsurface mixing in the hydrothermal system; 3) develop a schematic model of the hydrothermal system at Iheya North Knoll based on the stratigraphy, mineralogy, and geochemistry.

2. Geological setting and sample selection

The OT is a back arc basin (BAB) extending for about 1200 km between Kyushu Island and Taiwan. The north OT (NOT) is about 230 km wide with a maximum water depth of 200 m, and the south OT (SOT) is about 60–100 km wide with a maximum water depth of 2300 m (Letouzey and Kimura, 1986). The OT has been undergoing rifting since ~2 Ma, and was preceded by an earlier rifting episode during the Miocene

(Lee et al., 1980). Seismic reflection data suggest that the mantle (at ~ 6000 mbsf (meter below seafloor)) is overlain by potentially young basalt (~3000-6000 mbsf), igneous rocks (~ 1000-3000 mbsf), and sediments up to 1000 m thick (Expedition 331 Scientists, 2011). In 1988, Halbach et al. (1989) reported the occurrence of hydrothermal activity in the mid-OT. Thus far, at least six active hydrothermal fields have been identified: Minani-Ensei Knoll, Iheya North, Iheya Ridge, Izena Hole, Hatma Knoll, and Yonaguni Knoll IV (Takai et al., 2012).

The Iheya North Knoll (27°47′50″N, 126°53′80″E) is located approximately 150 km NNW of Okinawa Island (Fig. 1). Previous seismic and gravity core studies in the central valley of this hydrothermal field (apparent seafloor area as 2000 m×2000 m), suggested the presence of thick pumice layers with coarse to fine grain sizes, which often contain abundant gas-filled voids accompanied by elemental sulfur and sulfide minerals, probably deposited by gas-rich hydrothermal fluids (Oiwane, 2008; Expedition 331 Scientists, 2011; Masaki et al., 2011).

The samples selected for this study include sediments recovered from IODP 331 Sites C0013, C0014, C0015 C0016, C0017, as well as surface sediments and rocks collected in the north OT (NOT) during East China Sea (ECS) Investigation Expedition 2012 (Table 1). More detailed information about the cores is included in the IODP 331 report (Expedition 331 Scientists, 2011). A substantial amount of hydrothermally-formed secondary clay minerals, including chlorite, kaolinite-muscovite (intergrowth) and illite/smectite were recovered during IODP 331 Expedition (Expedition 331 Scientists, 2011; Miyoshi et al., 2015; Shao et al., 2015).

IODP Site C0016 is located at the base of the active (>310°C) hydrothermal vent

site and sulfide–sulfate mound at the North Big Chimney (NBC). Three cores were collected in Hole C0016B (no recovery in C0016A) over an interval of 0 to 45 mbsf, with a recovery of only 2.1 m (4.7%) of core. Core recovered from the 0–9 mbsf interval consists of massive and semi-massive sulfide underlain by silicified volcanic rock. The second core consists of only three rocks: two pieces of silicified volcaniclastic breccia and one piece of coarse anhydrite. The third core (27–45 mbsf) recovered ~1 m of quartz-chlorite-rich altered volcanic rock with abundant stock-work veining (Expedition 331 Scientists, 2011; Takai et al., 2012). For this study, we selected two samples from the first interval and one sample of white, coarsely crystalline anhydrite from the second interval (Table 1).

At IODP Site C0013, ~100 m east of NBC, four lithologic units were identified (Fig. 2). Unit I (0–4 mbsf): hydrothermally-altered mud containing crystalline pipes of elemental sulfur and sulfide grit; Unit II (4–14 mbsf): hydrothermally-altered mud with some heavily veined intervals and clastic units containing anhydrite breccia and fragments of metalliferous massive sulfide; Unit III (14–26 mbsf): hydrothermally-altered mud with abundant nodular anhydrite occurring in some layers; and Unit IV (26–55 mbsf): volcanic breccia with clasts of various volcanic rocks (Expedition 331 Scientists, 2011) (Fig. 2). Based on XRD data, the hydrothermally-altered mud is chlorite rich, up to 70% by volume (Miyoshi et al., 2015; Shao et al., 2015). For this study, twenty-four samples of the hydrothermally altered mud were selected between 0–26 mbsf.

IODP Site C0014 is located ~450 m east of NBC and is a region of relatively low surficial heat flow compared with Site C0013 (Fig. 2). The drilled sequence at this site represents deposition of hemipelagic and volcanoclastic materials that have been

subjected to hydrothermal alteration to different extents. The upper part (Unit I: 0 to <18 mbsf) shows little evidence of hydrothermal alteration and consists of a succession of hemipelagic oozes and coarse pumice gravel. The degree of hydrothermal alteration increases downward, showing partially consolidated hydrothermally-altered mud and coarse angular pumice gravel in Unit II (~12 to ~30 mbsf), and consolidated and often well-cemented volcanic sediments interbedded with hydrothermally-altered mud from ~30 to ~128 mbsf (Unit III). This site has much lower abundance of anhydrite than Site C0013, implying less direct seawater input into the system at this site or lower temperature (<150°C) (Humphris, 1998). The lower part of Unit III exhibits lower contents of chlorite but higher amounts of quartz and muscovite. In this study, we consider this part as Unit IV — a separate unit from Unit III, although they are classified as one unit in the IODP report (Expedition 331 Scientists, 2011). We analyzed 8 samples from Unit I, 8 from Unit II, 8 from Unit III, and 7 from Unit IV.

IODP Site C0017, located ~1550 m east of NBC, is inferred to be the recharge zone because of its low heat flow and low surficial thermal gradient (Fig.1; Expedition 331 Scientists, 2011). It mainly contains units of homogeneous hemipelagic mud, volcanoclastic–pumiceous breccia and mixed sand. No significant hydrothermal alteration was observed at this site, with the exception of weak alteration to clay within the deepest part (~150 mbsf) (Shao et al., 2015). The upper Unit I (0–28 mbsf) contains abundant foraminifera and coccoliths, suggesting a normal hemipelagic depositional environment (Expedition 331 Scientists, 2011; Shao et al., 2015). Pumiceous gravels dominate C0017-Unit II with interbedded detrital sediments, which has similar mineralogical characteristics to pumiceous sediments encountered at Site C0015. Because

of the similarity in sediment types, we combined Unit II and Unit III as described in the IODP report (Expedition 331 Scientists, 2011; Shao et al., 2015) into C0017-Unit II. The C0017-Unit III is dominated by hemipelagic mud, which corresponds to the Unit IV of IODP report (Expedition 331 Scientists, 2011; Shao et al., 2015).

IODP Site C0015 is located on a hill ~600 m northwest of NBC. Drilling reached only 9.4 mbsf and only two cores were recovered. They contain coarse pumiceous gravel and grit, siliciclastic sand, hemipelagic mud, bioclastic gravel, and foraminifera sediments. Pelagic sedimentation dominates at this site, but redeposited volcanic clasts comprise the bulk of the sediment (Expedition 331 Scientists, 2011). The C0015−Unit I mainly consists of hemipelagic mud, bioclastic and pumiceous sediment, while pumice gravels predominate C0015−Unit II. Overall, this site lacks obvious hydrothermal alteration.

The northern Okinawa Trough (NOT) has very thick sediments (up to 8 km thick) due to the supply of terrigenous material from the continent of China (Sibuet et al., 1987; Zhao et al., 1995; Wang et al., 2011; Yang et al., 2014). Hydrothermal activity in this region has been rarely reported. We selected 10 surficial sediment samples from the northern OT as representative of the terrigenous component input to the OT. In addition, one volcanic rock sample was selected as the fresh precursor rock prior to hydrothermal alteration.

3. Methods

X-ray diffraction (XRD) analyses were completed to determine the bulk mineralogy of the samples. They were performed on a Rigaku D/maxrB X-ray diffractometer (Cu-Kα radiation, 40 kV voltages; a 100 mA intensity and 2°/min (2θ) speed), with scanning

angles (2θ) varying from 3° to about 35°, following the method of Holtzapffel (1985). Identification of specific clay minerals was based on the basal layer plus the interlayer revealed by the XRD patterns (Brown and Brindley, 1980). The mineral contents (vol. %) were calculated using the software Siroquant V3. Similarly, the peak areas were calculated after manual baseline correction using MacDiff software version 4.2.2, following the semiquantitative method of Biscaye (1965). The error of this method is estimated to be about 5% of the relative abundance of each mineral (Biscaye, 1965). In this study, we did not process the samples with ethylene-glycol solvation and the "chlorite-rich" sediment should contain chlorite, smectite and/mixed-layer minerals.

The main purpose of this study is to investigate the origin of chlorite-rich sediments in mid-OT hydrothermal area. To separate the silicate fraction from the bulk samples and to minimize the dilution effect of biogenic components such as carbonates, we followed the 1 N HCl-leaching method in previous study (Shao et al., 2015) to process the bulk samples before the chemical digestion. The leaching process by 1 N HCl may greatly minimize the dilution effects of biogenic carbonates and some authigenic components (Choi et al., 2007; Dou et al., 2016), so the residues of hydrothermal sediments can better indicate the origins of chlorite-rich sediments relative to bulk samples. By doing so, we separated the leachable and residual phases, which may better discriminate the provenance and environmental signals registered in the bulk sediments. This leaching method was also applied for provenance studies of fluvial and marine sediments in East Asian continental margin (Yang et al., 2004; Choi et al., 2007; Song and Choi, 2009; Dou et al., 2016). About 0.5 g sample was leached with 25 ml 1N HCl for 24 hours at 50°C to separate the leachates and residues. The residues were rinsed with deionized water, and

then heated to dryness at 50°C. Because of the limited reaction time and low concentration of HCl, some sulfates and sulfides were likely retained in the residues. But most residues are mainly composed of silicate minerals, while leachates are mainly carbonates, sulfates, sulfides and minor silicate if any (Wang et al., 2015; Dou et al., 2016).

Measurements of major and trace elements were conducted on both leachates and residues. About 50 mg of the residues were digested with 1ml HNO_3 and 1ml HF for more than 48 hours in a tightly closed Teflon bomb in an oven at 190°C. After cooling, the bomb was evaporated at 120 °C to incipient dryness, then 1 ml HNO_3 was added, and evaporated again to dryness. The resultant solid was re-dissolved by adding 1 ml Milli Q-H_2O, 1 ml HNO_3, resealed and heated in the bomb at 190 °C for 12 hours. The final solution was transferred to a polyethylene bottle and diluted to ~100 g with 2% HNO_3, for elemental analyses by ICP-AES (IRIS Advantage) and ICP-MS (Agilent 7700e). The major elements were measured in the State Key Laboratory of Marine Geology at Tongji University, and the trace elements were analyzed in the Geochemical Laboratory of Wuhan Sample Solution Analysis Technology Co., LTD. The precision and accuracy were monitored by national geostandards GSR-5, GSR-6, and GSR-9 provided by the National Research Center. Based on the repetitive measurements of GSR-9, the analytic precision for most major and trace elements are 5–10%.

Fifty residue samples were analyzed for Sr-Nd isotopic ratios using a MC-ICP-MS (Neptune Plus, Thermo, Co.) in the Supergene Key Laboratory of the Ministry of Education, Nanjing University. Sr and Nd were separated and then collected using standard ion exchange techniques (Yang et al., 1997; Yang et al., 2007; Dou et al., 2016).

$^{87}Sr/^{86}Sr$ is normalized to $^{86}Sr/^{88}Sr$=0.1194 and $^{143}Nd/^{144}Nd$ to $^{146}Nd/^{144}Nd$=0.7219. The analytical blank was < 1 ng for Sr and < 60 pg for Nd, respectively. Reproducibility and accuracy of the Sr and Nd isotopic analyses were periodically checked by running the Sr standard NBS 987 and Nd standard AlphaNd, with a mean $^{87}Sr/^{86}Sr$ value of 0.710310 ± 0.00003 (2σ external standard deviation, n = 15) and mean $^{143}Nd/^{144}Nd$ value of 0.512270 ± 0.00002 (2σ external standard deviation, n = 6), respectively (Dou et al., 2016).

4. Results

The sediments in the mid-OT area are composed of terrigenous, biogenic, volcanic and hydrothermal sediments in variable proportions (Marumo and Hattori, 1999; Shinjo and Kato, 2000; Expedition 331 Scientists, 2011; Ishibashi et al., 2015). Samples selected from different components are shown in Table 2 and Appendix 1. In this section, we use the mineralogical and geochemical data of bulk samples to characterize each component.

4.1 Mineralogical compositions of bulk samples.

Figure 2 shows the mineralogical compositions of the cores determined from the XRD analysis.

4.1.1 Volcanic sediments/rocks, terrigenous sediments and biogenic components.

The upper parts (Unit I) of Sites C0014, C0015 and C0017 show little or no evidence for hydrothermal alteration and have mineralogy similar to the background sediments in the northern OT. Hemiplegic muds, pumiceous sediments, and volcanoclastic breccia comprise these sediments, and consist predominantly of detrital quartz, mica, feldspar and clay minerals with different proportions of calcium carbonate (Fig. 2). The carbonate (calcite) is mostly biogenic component in these units (Fig. 2), particularly in C0017-Unit I.

The pumiceous sediments in C0015-Unit II and the volcanic rock from north OT (NOT-Volcanic, Fig. 2) show feldspar-dominated mineral compositions (bulk sediment contains ~80% albite). Some layers in the C0017-Unit II contain abundant feldspar (e.g. anorthite), although this unit is mainly terrigenous minerals as in C0017-Unit I.

4.1.2 Hydrothermally altered sediments.

The hydrothermal sediments in this study have been grouped into four types based on the mineralogy and geochemistry (following section): mixed hydrothermal sediments, chlorite-rich sediments, anhydrite-rich sediments, and quartz-chlorite sediment/rock (Table 1; Fig. 2).

The mixed hydrothermal sediments (C0013-Unit I, C0014-Unit II and C0016-Unit I) show considerable heterogeneity in their mineralogy, consisting mainly of sulfides, sulfates, clay minerals, mica, and quartz in varying proportions (Fig. 2). Massive sulfides were recovered only in Unit I of Site C0016 located proximal to the active vent. However, veins and clastic units containing sulfides were observed at a depth of <9 mbsf in Site C0016 and also in Units I and II of C0013. Low-temperature secondary mineral assemblages (Expedition 331 Scientists, 2011) that include muscovite ± illite ± montmorillonite are present at all three locations (C0016-Unit 1; C0013-Unit I; and 14-Unit II). Some layers in C0013-Unit I and C0014-Unit II are dominated by kaolinite, which is observed at shallow depths or in close association with terrigenous sediment layers (Fig. 2).

In Unit III at Sites C0013 and C0014, chlorite is abundant and comprises up to 70% of the samples, accompanying sulfide (e.g. pyrite) and anhydrite (Fig. 2). Anhydrite-rich sediments are most abundant in C0013-Unit II and at a depth of ~12 mbsf in C0016 (Fig.

2). The quartz-chlorite sediment/rock occurs in both C0013-Unit IV and C0014-Unit IV, although C0014-Unit IV contains significant mica (muscovite), pyrite and anhydrite, which are either in trace amounts or absent C0013-Unit IV (Fig. 2).

4.2 Major, minor and rare earth element compositions of bulk samples

Figures 3 and 4 show the major and trace element compositions after normalization to upper continental crust (UCC) (Taylor and McLennan, 1985), and chondrite-normalized (Boynton, 1984) REE patterns in the residue and leachates of the bulk samples. The original data of all samples are shown in Appendix 2.

4.2.1 Volcanic sediments/rocks, terrigenous sediments and biogenic components.

The residues of Unit I in Sites C0014, C0015 and C0017 exhibit major and minor elemental compositions similar to the UCC and also to the NOT background samples. Except for the high Ca concentration in the leachate of Unit I in C0017, the background sediment samples show similar concentrations of major (e.g., Ca, Fe, Mg) and minor (e.g., Sr, Mn) elements with C0017-Unit I and C0014-Unit I (Figs. 3, 4). The residues of the samples studied, as well as the background sediment samples, have total concentrations of REE (ΣREE) mostly ranging from 59.7 to 157.6 ppm, and $(La/Yb)_N$ ratios of 5.4-10.4 (Table 2). In comparison, the leachates have considerably lower ΣREE, ranging from 24 to ~50 ppm (Table 2). The values of europium anomaly (δEu) are very similar in the residues and leachates, varying from 0.54 to 0.67.

The pumiceous sediments (C0015-Unit II) and the NOT-Volcanic sample exhibit similar geochemical patterns to that of UCC, but the pumice has higher contents of Zr, Hf, Y than the NOT-Volcanic sample (Fig. 3). The REE compositions of pumiceous sediment (C0015-Unit II) are significantly different from the NOT-Volcanic sample, yielding much

higher ΣREE and positive Eu anomalies in the residues (Fig. 4 and Table 2). C0017-Unit II is characterized by enriched light REE (LREEs) and flat patterns of heavy REEs (HREEs), but has higher ΣHREEs than terrigenous sediments in C0017-Unit I and Unit III.

4.2.2 Hydrothermally altered sediments.

Ta, Nb, Zr and Hf yield distinctly low concentrations in the leachates of almost all samples, but have slightly higher concentrations averaging UCC values in most residues of hydrothermal sediments (Fig. 3). The REEs tend to concentrate in the residues. The exception is the anhydrite sample from Site C0016 which has similar REE patterns in both residue and leachate fractions. In general, the residues of most samples show considerable LREE enrichment and flat patterns of HREEs with a negative Eu anomaly, while most leachates show enriched LREEs and depleted HREEs.

The sulfide-rich units in Sites C0013 and C0016 are characterized by distinctly high contents of Pb, Zn and Cu in both residues and leachates, as are the chlorite-rich sediments in Sites C0013 and C0014, likely due to the occurrence of disseminated fine-grained sulfides. However, the leachates and the residues of the coarsely crystalline anhydrite from Site C0016 show depletion in most elements relative to UCC, except for Sr and Ca. The ΣREE and chondrite-normalized (Boynton, 1984) patterns of C0016-Unit I (described as massive sulfide during IODP 331) are strikingly different from the other REE patterns, and is notable for its lower ΣREE, a relatively flat REE pattern with a weak Eu anomaly.

Unit I of C0013 and Unit II of C0014, which are dominated by low-temperature clay minerals, have ΣREE varying from 20.3 to 384 ppm in the residues, but all exhibit

LREEs enrichment, with mean $(La/Yb)_N$ ratios of 4.22 and 4.91 respectively. In comparison, the leachates of these samples have low ΣREE ranging from 0.22 to 58.73 ppm (Table 2), and considerably higher $(La/Yb)_N$ in C0013-Unit I (129.2 on average) than in C0014-Unit II (16.7 on average).

The chlorite-rich sediments (C0013-Unit III and C0014-Unit III) are characterized by high concentrations of Mg (8.2 wt% and 7.4 wt% in residues, respectively) and HREEs (Figs. 3, 4; Table 2). Although their absolute REE concentrations are higher, the $(La/Yb)_N$ ratios are similar to C0015-Unit II (Table 2). It is noteworthy that the mean δEu in C0013-Unit III (0.44 in the residues) is distinctly lower than in C0014-Unit III (0.53 on average) (Table 2).

The anhydrite sample from C0016 and the leachate of C0013-Unit II have similarly low REEs contents and flat LREE patterns with only a weak, if any, Eu anomaly (Fig. 4 and Table 2). C0013-Unit II contains anhydrite breccia and the similarity in REE patterns is likely a consequence of dissolution of anhydrite into the leachate when the sample was processed.

4.3 Sr and Nd isotopic compositions of bulk residual samples.

The Sr and Nd concentrations and isotopic compositions of the residues are shown in Figure 5 and Table 2. In some of the hydrothermally altered samples, the Sr concentrations were too low to permit Sr isotopic analyses. Please refer to Appendix 3 for the original data of all samples investigated.

The samples fall into distinct fields based on their origins or dominant mineralogy. The Sr isotopic ratios of all chlorite-rich sediments, apart from some samples of 14-Unit II, range between 0.7075 and 0.7100, being similar to the mean value of seawater ($^{87}Sr/^{86}Sr$

= 0.70916). They also exhibit high Nd concentrations and high values of εNd.

The unaltered samples of C0014-Unit I and from C0017 group together with the NOT background samples, showing relatively low concentrations of Sr and Nd, but high Sr and low Nd isotopic ratios.

Both Sr and Nd isotopic ratios in the anhydrite sample from C0016 are very close to those of seawater as expected (Fig. 5 and Table 2).

5. Discussion

5.1 The origin of chlorite-rich sediment in the mid-OT hydrothermal field

5.1.1 Evidence from high-field-strength element (HFSEs) contents and ratios.

Within submarine hydrothermal systems, the reactions between hydrothermal fluids, rocks and sediments exert important controls on the compositions of hydrothermal alteration products (Edmond et al., 1979; Thompson, 1983; Dekov et al., 2008; Miyoshi et al., 2013). During these processes, many elements are leached from the substrate, but some high-field-strength elements (HFSEs), such as Zr, Ti, Hf, Nb, Y, Th, are immobile and can become enriched in alteration mineral assemblages (MacLean and Kranidiotis, 1987; Karakaya et al., 2012). Furthermore, You et al. (1994; 1995; 1996) demonstrated that the incompatible elements (As, Be, Cs, Li, Pb, Rb), as well as the LREEs, are enriched in hydrothermal fluid at ~300℃. Hence, these elements may be important tracers to investigate the precursor of the hydrothermally altered sediments.

Figure 6a illustrates the enrichment of HFSEs and REEs in the chlorite-rich sediments (C0013-Unit III and C0014-Unit III) of the mid-OT, and shows that Zr and HREEs concentrations are about five times higher than in terrigenous and volcanic rocks/sediments. Note that C0015-Unit II, consisting of unaltered pumiceous gravel and

volcanic lithoclasts, has a distinctly higher content of Zr (up to 349 ppm) than other unaltered materials. In addition, the chlorite-rich sediments have significantly different geochemical compositions from the terrigenous sediments (Fig. 6b-d), indicating that the chlorite-rich sediments could not result from hydrothermal alteration of terrigenous sediments, and are likely derived from the alteration of volcanic materials. However, the considerable scatter of the data for the representative volcanic rocks from the OT (Fig. 6) does not allow us to clearly identify the type of volcanic material that was altered. Although the Eu anomalies overlap, the greater negative Eu anomaly of C0013 Unit III implies it underwent higher temperature alteration than C0014-Unit III, as Eu^{2+} occurs predominantly above ~250°C in natural hydrothermal systems (Alderton et al., 1980; Sverjensky, 1984; Wood, 1990b).

The volcanoclastic sediments recovered during Expedition 331 included pumiceous gravel and volcanoclastic breccia. Figure 7 shows the REE patterns for the two chlorite-rich sediment units normalized to the average REE compositions of C0015-Unit II that consists of an unaltered mixture of volcanic lithoclasts and pumiceous gravel. Although there is a slight depletion of LREEs relative to the unaltered volcanic materials (Fig. 7a), the REE patterns are generally flat. Previous studies have shown that during alteration of feldspar and other minerals, chlorite can accommodate HREEs more readily than the LREEs (MacLean and Kranidiotis, 1987).

Compared with chlorite-rich sediments from other sediment-covered or felsic-hosted hydrothermal systems (Goodfellow and Franklin, 1993; Goodfellow and Peter, 1994; Lackschewitz et al., 2000; Lackschewitz et al., 2004), the chlorite-rich sediments in the mid-OT are characterized by lower concentrations of Al and Fe but much higher Y, Zr, Hf,

Th and REEs, indicative of the distinct nature of the precursor rocks in this region.

5.1.2 Evidence from Nd isotopic compositions

At sites C0015 and C0017, the volcanoclastic materials are unaltered and hence should be representative of volcanic components emplaced in the mid-OT. However, the volcanoclastic materials recovered are mixed with terrigenous and biogenous sediments, and cannot be separated to serve as representative of the volcanic end member. Hence, other data for mid-OT rhyolite, andesite/basalt and pumice are included in Figures 5 and 6 for comparison (Shinjo, 1999; Shinjo et al., 1999; Shinjo and Kato, 2000).

The εNd values of chlorite-rich sediments are similar to those of pumice and andesite/basalt, but much higher than terrigenous sediments (Fig. 5), indicating these sediments likely resulted from alteration of volcanic rock rather than terrigenous sediments. The εNd in the residue of NOT-volcanic component is 1.2, which is similar to volcanic glasses (~1.6) collected in the mid-OT but different from the rhyolite and andesite/basalt collected in this area (Meng et al., 2001). This finding suggests that the NOT-volcanic sample and the mid-OT volcanic glasses might be produced during a similar volcanic eruption stage, although the NOT-volcanic rocks are not the precursors of mid-OT hydrothermal chlorite-rich sediments.

Derivation of the chlorite-rich sediment through alteration of mid-OT volcanic material is also supported by the similarity in εNd between the chlorite-rich sediments and the OT pumice and andesite/basalt (Fig. 5c) (Shinjo, 1999; Shinjo et al., 1999; Shinjo and Kato, 2000), although the Nd concentrations are distinctly higher in the chlorite-rich sediments. The lower and variable values of εNd in the upper units of both C0013 and C0014 reflects the interbedded terrigenous sediments and sulfides and or sulfates present

within the unit (Figs. 2, 5).

Very hard, highly altered volcanic breccia layers occurring at the bottom of C0016 and C0013 (Unit IV) have been interpreted to be volcanic basement (Expedition 331 Scientists, 2011). The quartz-chlorite sediment/rock occurs as C0014-Unit IV and C0013-Unit IV, but they show different REE patterns (lower ΣREEs and δEu, higher $(La/Yb)_N$ in C0013-Unit IV) (Fig. 4, Table 2). While εNd values show considerable scatter, C0014-Unit IV exhibits εNd values similar to those in the pumice and andesite/basalt, while C0013-Unit IV shows a higher εNd, suggesting they may be altered from different original materials (Fig. 5).

5.1.3 The transition from kaolinite-rich to chlorite-rich sediments with increasing depth

Kaolinite-rich layers in C0013-Unit I and C0014-Unit II are observed at shallow depths or in close association with terrigenous sediment layers (Fig. 2), and may be terrigenous or hydrothermal in origin. The presence of sulfides (galenite, sphalerite, etc.), sulfates, clays (kaolinite, illite, etc.) and other minerals in the mixed hydrothermal sediments suggests that these units were altered at lower temperatures of ~150−220°C (IODP Expedition 331 Scientists, 2011). In addition, the values of εNd are very close to the volcanic end members (pumice and andesite/basalt, etc.) (Fig. 5), suggesting that these kaolinite-rich layers resulted from hydrothermal alteration of volcanic materials.

The kaolinite-rich sediment shows LREEs enrichment relative to chlorite-rich sediments, indicating that LREEs may be leached during high temperature alteration or added to the kaolinite sediments during lower temperature alteration (Figs. 4, 7). However, the overall REE patterns of these altered sediments vary within a similar range to pumiceous sediments (C0015-Unit II) (Fig. 7b). Hence, the kaolinite-rich sediment

may result from lower-grade alteration of pumiceous material, while chlorite-rich sediment represents the product of higher-grade alteration (consistent with temperatures of ~220−300°C (Expedition 331 Scientists, 2011).

Chemical conditions, in addition to temperature, control the types of clay mineral formation. Hydrothermal kaolinite reflects fluids of low pH and low Mg (Huertas et al., 1999; Haile et al., 2015), while chlorite and smectite are commonly formed in Mg-bearing and high pH fluid conditions (Howard and Fisk, 1988; Haile et al., 2015). The low concentration of Mg in kaolinite-rich sediment (Appendix 2), together with the occurrence of native sulfur and sulfate (as well as high H_2S in the pore-water and sediments) near the kaolinite-rich layers (IODP Expedition 331 Scientists, 2011), suggest that kaolinite precipitated from acidic fluids with a small quantity of seawater entrainment. Note that the discharging hydrothermal fluid has a pH of ~5 (NBC) (Ishibashi et al., 2015), reflecting the acidic condition at Iheya North Knoll.

The occurrence of Mg-chlorite at lower parts of sites C0013 and C0014 indicates seawater was entrained into the subsurface (Fig. 2 and Appendix 2) (IODP Expedition 331 Scientists, 2011). The Sr isotopes of anhydrite overlying on the chlorite-rich sediment also support seawater entrainment (detailed discussion in section 5.2).

Note that Unit I of C0014 is unaltered, which is likely due to the presence of an impermeable hard layer between Unit I and Unit II (Expedition 331 Scientists, 2011). Indeed, at least three impermeable layers between different units of site C0013 and C0014 have been identified (Expedition 331 Scientists, 2011; Miyoshi et al., 2015).

5.1.4 Alternative process of chlorite formation

The similarity in geochemical and isotopic data for the chlorite-rock sediments

comprising C0013-Unit III and C0014-Unit III (Figs. 4 and 5) indicate hydrothermal alteration under similar conditions at both locations. Laboratory studies have shown that there is very rapid nucleation and growth of a clay coating (smectite, chlorite) on the surfaces of clean feldspar and quartz grains at hydrothermal (100–150°C) conditions with high pH (≥5.66) and Mg content (Haile et al., 2015), and that the thickness of the coating increases with increasing temperature and reaction rate. In the mid-OT hydrothermal system, where temperatures are >300°C and the pumiceous gravel and volcanic lithoclasts are dominated by feldspar, the alteration conditions may favor the formation of chlorite-rich sediments.

An alternative mechanism of chlorite formation, i.e. the dissolution of illite at temperatures of 200°C, has been suggested by Miyoshi et al. (2015) based on studies in the same area. Illite is a common component of terrigenous sediment in the mid-OT, so formation of chlorite-rich sediments in some parts of the hydrothermal system by this mechanism cannot be ruled out. The dissolution of illite produces both chlorite and quartz, which has been observed in some samples (Fig. 2). However, the lack of a significant component of quartz in C0013-Unit III and C0014-Unit III, together with the geochemical and isotopic data discussed above, suggests that these layers resulted predominantly from hydrothermal alteration of volcanic material, rather than from the alteration of siliciclastic sediments.

5.2 The formation of anhydrite in the mid-OT sediments

Anhydrite, which exhibits retrograde solubility, is the most important sulfate phase at the mid-OT hydrothermal area, although barite has been observed in some layers (Fig. 2). Substantial amounts of anhydrite were identified in C0013-Unit II and in the lower part

of C0016. This is indicative of entrainment of seawater into the subsurface, followed by precipitation of anhydrite from either conductive heating of seawater, or from mixing with high-temperature hydrothermal fluid, to temperatures >150°C (Mills and Elderfield, 1995; Humphris, 1998; Humphris and Bach, 2005; Craddock et al., 2010).

5.2.1 Behavior of REEs in the formation of anhydrite

Previous studies of anhydrite from hydrothermal systems on sediment-starved mid-ocean ridges have indicated that anhydrite precipitation causes measurable removal of aqueous REEs during fluid mixing, and that there is little fractionation of REEs except for Eu (Mitra et al., 1994; Mills and Elderfield, 1995; Meng et al., 2001; Bach et al., 2003; Craddock et al., 2010). Hence, the chondrite-normalized (Boynton, 1984) REE patterns for anhydrite from sediment-starved mid-ocean ridges often reflect that of the fluid from which anhydrite precipitated.

The anhydrites analyzed in this study exhibit different REEs patterns from the OT end-member hydrothermal fluids data of Hongo et al. (2007). They show enrichments in LREEs relative to the HREEs (Fig. 8) but not such strong enrichments as observed in the hydrothermal fluids (Hongo et al., 2007). The relative LREEs depletion likely results from the presence of stable LREE chloro-complexes that limit the availability of the LREEs from partitioning into the anhydrite (Wood, 1990b). This factor may also explain the differences in LREE enrichments between the two sites. The relatively lower temperature (~150 – ~220°C) (Expedition 331 Scientists, 2011) in C0013-Unit II may reduce the stability of LREE chloro-complexes in the fluids, allowing more partitioning into the anhydrite. In contrast, the C0016-Anhydrite REE pattern exhibits less REEs enrichment so it likely precipitated from higher temperature fluids in which the chloro-

complexes were more stable.

In addition, the Eu anomaly is slightly negative in the OT anhydrites compared to being strongly positive in the fluids (Fig. 8). These REE patterns are very similar to that of anhydrite from a black smoker chimney from the TAG hydrothermal area, Mid-Atlantic Ridge (Mills and Elderfield, 1995), and some anhydrite samples recovered from the subsurface of the TAG active mound (Humphris, 1998). This is likely due to the presence of only Eu^{2+} at temperatures above 250°C and the mismatch in ionic radii between Eu^{2+} and Ca^{2+}, as well as the strong chloro-complexation of Eu^{2+} which inhibits partitioning of Eu^{2+} into anhydrite (Shannon, 1976; Wood, 1990b; Humphris and Bach, 2005).

The consistent depth of occurrence of coarse anhydrite at Sites C0013 and C0016 may reflect the presence of a wide anhydrite-rich zone that was sampled at both sites (Fig. 2) (Expedition 331 Scientists, 2011). Although Sr isotopic compositions have not been analyzed in anhydrite-dominated leachates from C0013-Unit II, the similarities of elemental concentrations and REE patterns observed in the units at C0013 and C0016 may reflect very similar seawater/fluid ratios during anhydrite formation (Figs. 3, 4, 8). However, the difference in magnitude of the anhydrite Eu anomaly between the two sites may indicate different temperatures of formation (Fig. 8).

5.2.2 Sr isotopic composition of anhydrite

The Sr isotopic composition of anhydrite records the extent of mixing between hydrothermal fluids and seawater (Albarède et al., 1981; James and Elderfield, 1996). The anhydrite from Site C0016, which is 20 m from the active vent most likely within the upflow zone, is coarsely crystalline and provides an opportunity to gain some insight into

the amount of seawater entrainment into the upper part of the hydrothermal system.

We have used a simple mass balance to estimate the proportion of seawater-derived Sr in the C0016 anhydrite. We assume that the only source for Sr in the hydrothermal fluids are volcanic rock and seawater (it does not include the terrigenous sediment as a potential source of Sr). We used the average $^{87}Sr/^{86}Sr$ (0.70365) in Central Ryukyu andesite/basalt and pumice (Shinjo, 1999; Shinjo and Kato, 2000) (Fig. 5) as representative of the starting volcanic rock, and the $^{87}Sr/^{86}Sr$ ratio in modern seawater (0.70916) (Richter et al., 1992). The $^{87}Sr/^{86}Sr$ ratio (0.70882) of the anhydrite from C0016 suggests that the contribution of seawater-derived Sr accounts for about 94% of the Sr in the anhydrite. Hence, seawater entrainment is a significant process within the upflow zone of the Iheya hydrothermal system, and the entrained seawater must have undergone conductive heating.

6. A schematic model for the mid-Okinawa Trough hydrothermal system

Figure 9 presents a schematic diagram for the mid-OT hydrothermal system based on interpretation of the mineralogy and geochemistry of the sediments and volcanoclastic material. The OT receives a great amount of terrigenous sediments from continents, but there is also an important input of volcanic materials (Fig. 9a). The substrate at Iheya North Knoll was likely composed of pumiceous sediments and other volcanoclastic materials interbedded with hemipelagic (terrigenous and biogenous) sediments. Impermeable layers (red boundaries) separated some units (Expedition 331 Scientists, 2011; Miyoshi et al., 2015), thereby influencing hydrothermal fluid flow and resulting in variable degrees and types of hydrothermal alteration within different units (Fig. 9b). Based on the REEs and isotopes, the chlorite-rich and kaolinite-rich layers resulted from

alteration of the pumiceous material at higher and lower temperatures respectively. Seawater entrainment and subsurface mixing, and the precipitation of anhydrite, is an important process at Sites C0016 and C0013.

In summary, it is clear that the substrate at Iheya North Knoll has played a significant role in determining the hydrothermal mineral assemblages produced in this back-arc basin area. We conclude that the chlorite- and kaolinite-rich sediments were formed from hydrothermal alteration of pumiceous (volcanic) materials. Based on the new isotopic data, as well as the inclusion of pumiceous sediment in the samples analyzed, this revises the conclusion of Shao et al. (2015) who inferred a detrital origin for the hydrothermal clays found in the North Iheya Knoll hydrothermal field.

Acknowledgements

This work was supported by the National Natural Science Foundation of China (Grant Nos. 41376049 and 41225020), National Programme on Global Change and Air-Sea Interaction (GASI-GEOGE-03), AoShan Talents Program Supported by Qingdao National Laboratory for Marine Science and Technology (No. 2015ASTP-OS11), Program of Shanghai Subject Chief Scientist (No. 14XD1403600), and Continental Shelf Drilling Program (No. GZH201100202). We thank all on-board scientists and crew for their help during IODP Expedition 331. Special thanks go to the China Scholarship Council (CSC) which funded Hebin Shao to visit Woods Hole Oceanographic Institution for one year. This work benefited from discussions with Sune Nielsen. Thanks also to Jeff Alt and Wolfgang Bach who provided constructive reviews.

References

Albarède, F., Michard, A., Minster, J.F., Michard, G., 1981. $^{87}Sr/^{86}Sr$ ratios in hydrothermal waters and deposits from the East Pacific Rise at 21°N. Earth Planet. Sci. Lett. , 55(2): 229−236.

Alderton, D.H.M., Pearce, J.A., Potts, P.J., 1980. Rare earth element mobility during granite alteration: Evidence from southwest England. Earth Planet. Sci. Lett. , 49(1): 149−165.

Alibo, D.S., Nozaki, Y., 1999. Rare earth elements in seawater: particle association, shale-normalization, and Ce oxidation. Geochim. Cosmochim. Acta 63(3–4): 363−372.

Alt, J., 1999. Very Low-Grade Hydrothermal Metamorphism of Basic Igneous Rocks. Low-grade metamorphism: 169−201.

Bach, W., Roberts, S., Vanko, D.A., Binns, R.A., Yeats, C.J., Craddock, P.R., Humphris, S.E., 2003. Controls of fluid chemistry and complexation on rare-earth element contents of anhydrite from the Pacmanus subseafloor hydrothermal system, Manus Basin, Papua New Guinea. Miner. Deposita 38(8): 916−935.

Beaufort, D., Rigault, C., Billon, S., Billault, V., Inoue, A., Inoue, S., Patrier, P., 2015. Chlorite and chloritization processes through mixed-layer mineral series in low-temperature geological systems–a review. Clay Minerals, 50(4): 497−523.

Biscaye, P.E., 1965. Mineralogy and sedimentation of recent deep-sea clay in the Atlantic Ocean and adjacent seas and oceans. Geol. Soc. Am. Bull. , 76(7): 803−832.

Bouvier, A., Vervoort, J.D., Patchett, P.J., 2008. The Lu–Hf and Sm–Nd isotopic composition of CHUR:Constraints from unequilibrated chondrites and implications for the bulk composition of terrestrial planets. Earth Planet. Sci. Lett.,

273(1–2): 48−57.

Boynton, W.V., 1984. Chapter 3–Cosmochemistry of the Rare Earth Elements: Meteorite Studies. Developments in Geochemistry, 2(2): 63−114.

Brown, G., Brindley, G., 1980. X-ray diffraction procedures for clay mineral identification. Crystal structures of clay minerals and their X-ray identification, 5: 305−359.

Chen, J., Li, G., Yang, J., Rao, W., Lu, H., Balsam, W., Sun, Y., Ji, J., 2007. Nd and Sr isotopic characteristics of Chinese deserts: Implications for the provenances of Asian dust. Geochim. Cosmochim. Acta 71(15): 3904-3914.

Choi, M.-S., Yi, H.-I., Yang, S.Y., Lee, C.-B., Cha, H.-J., 2007. Identification of Pb sources in Yellow Sea sediments using stable Pb isotope ratios. Mar. Chem. , 107(2): 255−274.

Craddock, P.R., Bach, W., Seewald, J.S., Rouxel, O.J., Reeves, E., Tivey, M.K., 2010. Rare earth element abundances in hydrothermal fluids from the Manus Basin, Papua New Guinea: Indicators of sub-seafloor hydrothermal processes in back-arc basins. Geochim. Cosmochim. Acta 74(19): 5494−5513.

Dekov, V., Cuadros, J., Shanks, W., Koski, R., 2008. Deposition of talc-kerolite-smectite-smectite at seafloor hydrothermal vent fields: Evidence from mineralogical, geochemical and oxygen isotope studies. Chem. Geol. , 247(1−2): 171−194.

Dekov, V., Scholten, J., Botz, R., Garbe-Schönberg, C.-D., Thiry, M., Stoffers, P., Schmidt, M., 2005. Occurrence of kaolinite and mixed-layer kaolinite/smectite in hydrothermal sediments of Grimsey Graben, Tjörnes Fracture Zone (north of Iceland). Mar. Geol. , 215(3): 159−170.

Dou, Y.G., Yang, S.Y., Shi, X.F., Clift, P.D., Liu, S.F., Liu, J.H., Li, C., Bi, L., Zhao, Y.,

2016. Provenance weathering and erosion records in southern Okinawa Trough sediments since 28 ka: geochemical and Sr-Nd-Pb isotopic evidences. Chem. Geol. 425: 93−109

Edmond, J.M., Measures, C., McDuff, R., Chan, L., Collier, R., Grant, B., Gordon, L., Corliss, J., 1979. Ridge crest hydrothermal activity and the balances of the major and minor elements in the ocean: The Galapagos data. Earth Planet. Sci. Lett. , 46(1): 1−18.

Expedition 331 Scientists, 2011. Expedition 331 summary. In Takai, K., Mottl, M.J., Nielsen, S.H., and the Expedition 331 Scientists, Proc. IODP, 331: Tokyo (Integrated Ocean Drilling Program Management International, Inc.).

Glasby, G.P., Notsu, K., 2003. Submarine hydrothermal mineralization in the Okinawa Trough, SW of Japan: an overview. Ore Geol. Rev. , 23(3–4): 299−339.

Goodfellow, W.D., Franklin, J.M., 1993. Geology, Mineralogy, and Chemistry of Sediment-Hosted Clastic Massive Sulfides in Shallow Cores, Middle Valley, Northern Juan de Fuca Ridgeii. Geology, 88: 2037−2068.

Goodfellow, W.D., Peter, J.M., 1994. 11. Geochemistry of hydrothermal altered sediment, Middle Valley, Northern Juan de Fuca Ridge 1, 2. In: Mottl, M.J., Davis, E.E., Fisher, A.T., and Slack, J.F. (Eds.), Proceedings of the Ocean Drilling Program, Scientific Results, 13: 207−289.

Haile, B.G., Hellevang, H., Aagaard, P., Jahren, J., 2015. Experimental nucleation and growth of smectite and chlorite coatings on clean feldspar and quartz grain surfaces. Mar. Pet. Geol. , 68, Part A: 664−674.

Halbach, P., Nakamura, K.-i., Wahsner, M., Lange, J., Sakai, H., Käselitz, L., Hansen, R.-

D., Yamano, M., Post, J., Prause, B., 1989. Probable modern analogue of Kuroko-type massive sulphide deposits in the Okinawa Trough back-arc basin. Nature, 338(6215): 496−499.

Herzig, P.M., Hannington, M.D., 1995. Polymetallic massive sulfides at the modern seafloor a review. Ore Geol. Rev. , 10(2): 95−115.

Herzig, P.M., Hannington, M.D., 2000. Polymetallic massive sulfides and gold mineralization at mid-ocean ridges and in subduction-related environments. Handbook of marine mineral deposits: 347−368.

Holtzapffel, T., 1985. Les minéraux argileux: préparation, analyse diffractométrique et détermination, 12. Société géologique du Nord.

Hongo, Y., Obata, H., Gamo, T., Nakaseama, M., Ishibashi, J., Konno, U., Saegusa, S., Ohkubo, S., Tsunogai, U., 2007. Rare Earth Elements in the hydrothermal system at Okinawa Trough back-arc basin. Geochem. J. , 41(1): 1−15.

Howard, K.J., Fisk, M.R., 1988. Hydrothermal alumina-rich clays and boehmite on the Gorda Ridge. Geochim. Cosmochim. Acta. 52, 2269– 2279.

Huertas, F.J., Fiore, S., Huertas, F., Linares, J., 1999. Experimental study of the hydrothermal formation of kaolinite. Chem. Geol. 156, 171– 190.

Humphris, S.E., 1998. Rare earth element composition of anhydrite: implications for deposition and mobility within the active TAG hydrothermal mound, PROCEEDINGS-OCEAN DRILLING PROGRAM SCIENTIFIC RESULTS. NATIONAL SCIENCE FOUNDATION, pp. 143−162.

Humphris, S.E., Bach, W., 2005. On the Sr isotope and REE compositions of anhydrites from the TAG seafloor hydrothermal system. Geochim. Cosmochim. Acta, 69 (6):

1511−1525.

Ishibashi, J.-i., Okino, K., Sunamura, M., 2015. Subseafloor Biosphere Linked to Hydrothermal Systems. Springer.

James, R.H., Elderfield, H., 1996. Chemistry of ore-forming fluids and mineral formation rates in an active hydrothermal sulfide deposit on the Mid-Atlantic Ridge. Geology, 24(12): 1147−1150.

Karakaya, M.Ç., Karakaya, N., Küpeli, Ş., Yavuz, F., 2012. Mineralogy and geochemical behavior of trace elements of hydrothermal alteration types in the volcanogenic massive sulfide deposits, NE Turkey. Ore Geol. Rev., 48: 197−224.

Kawagucci, S., Chiba, H., Ishibashi, J.-i., Yamanaka, T., Toki, T., Muramatsu, Y., Ueno, Y., Makabe, A., Inoue, K., Yoshida, N., 2011. Hydrothermal fluid geochemistry at the Iheya North field in the mid-Okinawa Trough: Implication for origin of methane in subseafloor fluid circulation systems, 45: 109−124.

Lackschewitz, K., Singer, A., Botz, R., Garbe-Schönberg, D., Stoffers, P., Horz, K., 2000. Formation and transformation of clay minerals in the hydrothermal deposits of Middle Valley, Juan de Fuca Ridge, ODP Leg 169. Economic Geology, 95(2): 361−389.

Lackschewitz, K.S., Devey, C.W., Stoffers, P., Botz, R., Eisenhauer, A., Kummetz, M., Schmidt, M., Singer, A., 2004. Mineralogical, geochemical and isotopic characteristics of hydrothermal alteration processes in the active, submarine, felsic-hosted PACMANUS field, Manus Basin, Papua New Guinea. Geochim. Cosmochim. Acta 68(21): 4405−4427.

Lee, C.-S., Shor, G.G., Bibee, L.D., Lu, R.S., Hilde, T.W.C., 1980. Regional geophysical

studies associated with IPOD site surveys Okinawa Trough: Origin of a back-arc basin. Mar. Geol. , 35(1): 219−241.

Letouzey, J., Kimura, M., 1986. Geodynamics of the Eurasia\3-Philippine Sea Plate Boundary The Okinawa Trough: Genesis of a back-arc basin developing along a continental margin. Tectonophysics, 125(1): 209−230.

MacLean, W., Kranidiotis, P., 1987. Immobile elements as monitors of mass transfer in hydrothermal alteration; Phelps Dodge massive sulfide deposit, Matagami, Quebec. Economic Geology, 82(4): 951−962.

Marumo, K., Hattori, K.H., 1999. Seafloor hydrothermal clay alteration at Jade in the back-arc Okinawa Trough: Mineralogy, geochemistry and isotope characteristics. Geochim. Cosmochim. Acta 63(18): 2785−2804.

Masaki, Y., Kinoshita, M., Inagaki, F., Nakagawa, S., Takai, K., 2011. Possible kilometer-scale hydrothermal circulation within the Iheya-North field, mid-Okinawa Trough, as inferred from heat flow data. JAMSTEC Report of Research and Development, 12: 1−12.

Meng, X.-W., Du, D.-W., Wu, J.-L., 2001. Quantitative Partition of Mixed Surface Sediments from the Middle Okinawa Trough into Their End-Members Using Sr-Nd Isotope. Oceanologia et Limnologia Sinica, 32(3): 326−332.

Mills, R.A., Elderfield, H., 1995. Rare earth element geochemistry of hydrothermal deposits from the active TAG Mound, 26°N Mid-Atlantic Ridge. Geochim. Cosmochim. Acta 59(17): 3511−3524.

Mitra, A., Elderfield, H., Greaves, M., 1994. Rare earth elements in submarine hydrothermal fluids and plumes from the Mid-Atlantic Ridge. Mar. Chem. , 46(3):

217−235.

Miyoshi, Y., Ishibashi, J.-i., Faure, K., Maeto, K., Matsukura, S., Omura, A., Shimada, K., Sato, H., Sakamoto, T., Uehara, S., Chiba, H., Yamanaka, T., 2013. Mg-rich clay mineral formation associated with marine shallow-water hydrothermal activity in an arc volcanic caldera setting. Chem. Geol. , 355: 28−44.

Miyoshi, Y., Ishibashi, J.i., Shimada, K., Inoue, H., Uehara, S., Tsukimura, K., 2015. Clay Minerals in an Active Hydrothermal Field at Iheya - North - Knoll, Okinawa Trough. Resource Geology, 65(4): 346-360.

Oiwane, H., Kumagai, Y., Nakamura, Y., and Tokuyama, H., 2008. Characteristics of sediment in Iheya North Knoll an“the acoustic blanking layer.”. JPGU Meeting, Abstract: J164−P013.

Piepgras, D.J., Wasserburg, G., Dasch, E., 1979. The isotopic composition of Nd in different ocean masses. Earth Planet. Sci. Lett. , 45(2): 223−236.

Richter, F.M., Rowley, D.B., DePaolo, D.J., 1992. Sr isotope evolution of seawater: the role of tectonics. Earth Planet. Sci. Lett. , 109(1–2): 11−23.

Shannon, R.t., 1976. Revised effective ionic radii and systematic studies of interatomic distances in halides and chalcogenides. Acta Crystallographica Section A: Crystal Physics, Diffraction, Theoretical and General Crystallography, 32(5): 751−767.

Shao, H., Yang, S., Wang, Q., Guo, Y., 2015. Discriminating hydrothermal and terrigenous clays in the Okinawa Trough, East China Sea: Evidences from mineralogy and geochemistry. Chem. Geol. , 398: 85−96.

Shinjo, R., 1999. Geochemistry of high Mg andesites and the tectonic evolution of the Okinawa Trough–Ryukyu arc system. Chem. Geol. , 157(1–2): 69−88.

Shinjo, R., Chung, S.L., Kato, Y., Kimura, M., 1999. Geochemical and Sr-Nd isotopic characteristics of volcanic rocks from the Okinawa Trough and Ryukyu Arc: Implications for the evolution of a young, intracontinental back arc basin. J. Geophys. Res. , 104(B5): 10591–10608.

Shinjo, R., Kato, Y., 2000. Geochemical constraints on the origin of bimodal magmatism at the Okinawa Trough, an incipient back-arc basin. Lithos, 54(3–4): 117−137.

Sibuet, J.C., Letouzey, J., Barbier, F., Charvet, J., Foucher, J.P., Hilde, T.W., Kimura, M., Chiao, L.Y., Marsset, B., Muller, C., 1987. Back arc extension in the Okinawa Trough. Journal of Geophysical Research: Solid Earth (1978–2012), 92(B13): 14041−14063.

Song, Y.H., Choi, M.S., 2009. REE geochemistry of fi ne-grained sediments from major rivers around the Yellow Sea. Chem. Geol. 266, 337–351.

Sverjensky, D.A., 1984. Europium redox equilibria in aqueous solution. Earth Planet. Sci. Lett. , 67(1): 70−78.

Takai, K., Mottl, M.J., Nielsen, S.H., 2012. IODP Expedition 331: Strong and Expansive Subseafloor Hydrothermal Activities in the Okinawa Trough. Scientific drilling(13): 19−27.

Taylor, S.R., McLennan, S.M., 1985. The Continental Crust: Its Composition and Evolution. Blackwell Sci.: 312.

Teagle, D.A.H., Alt, J.C., Chiba, H., Humphris, S.E., Halliday, A.N., 1998a. Strontium and oxygen isotopic constraints on fluid mixing, alteration and mineralization in the TAG hydrothermal deposit. Chem. Geol. , 149(1–2): 1−24.

Teagle, D.A.H., Alt, J.C., Halliday, A.N., 1998b. Tracing the chemical evolution of fluids

during hydrothermal recharge: Constraints from anhydrite recovered in ODP Hole 504B. Earth Planet. Sci. Lett. , 155(3–4): 167−182.

Thompson, G., 1983. Hydrothermal fluxes in the ocean. Chemical oceanography, 8: 271−337.

Wang, H., Saito, Y., Zhang, Y., Bi, N., Sun, X., Yang, Z., 2011. Recent changes of sediment flux to the western Pacific Ocean from major rivers in East and Southeast Asia. Earth Sci. Rev. , 108(1−2): 80−100.

Wang, S.-J., Teng, F.-Z., Rudnick, R.L., Li, S.-G., 2015. The behavior of magnesium isotopes in low-grade metamorphosed mudrocks. Geochim. Cosmochim. Acta 165: 435−448.

Wood, S.A., 1990b. The aqueous geochemistry of the rare-earth elements and yttrium. Chem. Geol. , 88(1): 99−125.

Yang, J., Tao, X., Xue, Y., 1997. Nd isotopic variations of Chinese seawater during Neoproterozoic through Cambrian. Chem. Geol. , 135(1): 127−137.

Yang, S.Y., Lim, D.I., Jung, H.S., Oh, B.C., 2004. Geochemical composition and provenance discrimination of coastal sediments around Cheju Island in the southeastern Yellow Sea. Mar. Geol. , 206(1–4): 41−53.

Yang, S., Jiang, S., Ling, H., Xia, X., Sun, M., Wang, D., 2007. Sr-Nd isotopic compositions of the Changjiang sediments: Implications for tracing sediment sources. Science in China Series D: Earth Sciences, 50(10): 1556−1565.

Yang, S., Wang, Z., Dou, Y., Shi, X., 2014. A review of sedimentation since the Last Glacial Maximum on the continental shelf of eastern China. Geological Society, London, Memoirs, 41(1): 293−303.

You, C.-F., Chan, L., Spivack, A., Gieskes, J., 1995. Lithium, boron, and their isotopes in sediments and pore waters of Ocean Drilling Program Site 808, Nankai Trough: implications for fluid expulsion in accretionary prisms. Geology, 23(1): 37−40.

You, C.-F., Morris, J., Gieskes, J., Rosenbauer, R., Zheng, S., Xu, X., Ku, T., Bischoff, J., 1994. Mobilization of beryllium in the sedimentary column at convergent margins. Geochim. Cosmochim. Acta 58(22): 4887−4897.

You, C.F., Castillo, P.R., Gieskes, J.M., Chan, L.H., Spivack, A.J., 1996. Trace element behavior in hydrothermal experiments: Implications for fluid processes at shallow depths in subduction zones. Earth Planet. Sci. Lett. , 140(1–4): 41−52.

Zhao, Y.-Y., Jiang, R.-H., Yan, M.-C., 1995. Abundance of chemical elements in continental shelf sediment of China. Geo-Mar. Lett. , 15(2): 71−76.

Table 1 The inventory of samples in this study (see details in IODP Report by Expedition 331 Scientists (2011)).

IODP 331 sample numbers	Samples	Top depth (mbsf)	Depth interval (cm)	Comments	Types
C0013F-1H-1 W, 2.0--4.0 cm	13-Unit I	0.02	2		
C0013B-1T-1 W, 3.5--5.5 cm	13-Unit I	0.04	2		
C0013B-1T-1 W, 17.5--19.5 cm	13-Unit I	0.18	2	Hydrothermally altered mud, sand, and grit with unconsolidated medium- to coarse-grained hydrothermal sulfide lithoclasts.	Hydrothermally altered sediments
C0013F-1H-3 W, 6.0--8.0 cm	13-Unit I	1.25	2		
C0013F-1H-3 W, 92.0--94.0 cm	13-Unit I	2.11	2		
C0013F-1H-5 W, 10.0--12.0 cm	13-Unit I	3.26	2		
C0013C-1H-2 W, 70.0--72.0 cm	13-Unit I	4.15	2		
C0013E-1H-6 W, 33.0--35.0 cm	13-Unit II	5.04	2		
C0013D-1H-4 W, 104.0--106.0 cm	13-Unit II	7.25	2		
C0013F-1H-CC W, 34.0--36.0 cm	13-Unit II	8.52	2	Hydrothermally altered mud with some heavily veined intervals, as well as coarser lithologies containing anhydrite and detrital metalliferous massive sulfide lithoclasts	Hydrothermally altered sediments
C0013C-1H-13 W, 92.0--94.0 cm	13-Unit II	10.05	2		
C0013C-1H-14 W, 28.5--30.5 cm	13-Unit II	10.87	2		
C0013C-1H-16 W, 40.0--42.0 cm	13-Unit II	12.20	2		
C0013D-2H-1 W, 10.0--12.0 cm	13-Unit II	12.60	2		
C0013D-2H-1 W, 51.0--53.0 cm	13-Unit III	13.01	2		
C0013D-2H-2 W, 42.0--44.0 cm	13-Unit III	13.94	2	Hydrothermally altered mud with layers rich in nodular anhydrite which is distinguished from Unit II by the presence of large polycrystalline anhydrite nodules and reduced abundances of clear vein anhydrite. Major altered minerals are anhydrite, illite, and Mg chlorite.	Hydrothermally altered sediments
C0013D-2H-3 W, 40.0--42.0 cm	13-Unit III	14.92	2		
C0013E-5H-1 W, 18.5--20.5 cm	13-Unit III	16.19	2		
C0013E-5H-1 W, 54.0--56.0 cm	13-Unit III	16.54	2		
C0013E-5H-1 W, 73.5--75.5 cm	13-Unit III	16.74	2		
C0013D-2H-5 W, 59.0--61.0 cm	13-Unit III	17.02	2		
C0013D-2H-6 W, 55.0--57.0 cm	13-Unit III	18.38	2		
C0013D-3T-1 W, 30.0--32.0 cm	13-Unit III	22.30	2		
C0013E-7L-1 W, 21.0--23.0 cm	13-Unit IV	26.21	2	Silicified volcanic breccia. Major minerals are Quatz and Mg-chlorite.	Hydrothermally altered sediments
C0014G-1H-1 W, 2.0--4.0 cm	14-Unit I	0.02	2		
C0014B-1H-1 W, 8.0--10.0 cm	14-Unit I	0.08	2		
C0014G-1H-1 W, 15.0--17.0 cm	14-Unit I	0.15	2	Hemipelagic homogeneous mud—silty clay to clayey silt, and characterized by abundant microfossils; and angular clasts of woody pumice	Terrigenous and biological sediments
C0014G-1H-1 W, 120.0--122.0 cm	14-Unit I	1.20	2		
C0014B-1H-2 W, 10.0--12.0 cm	14-Unit I	1.52	2		
C0014G-1H-3 W, 25.0--27.0 cm	14-Unit I	3.08	2		
C0014B-1H-5 W, 42.0--44.0 cm	14-Unit I	6.06	2		
C0014B-2H-3 W, 70.0--72.0 cm	14-Unit I	9.27	2		
C0014B-2H-6 W, 55.0--57.0 cm	14-Unit II	12.32	2	Hydrothermally altered mud, mud, and sand with detrital hydrothermal component, and sulfidic sediment. Major minerals are	Hydrothermally altered sediments
C0014B-2H-12 W, 50.0--52.0 cm	14-Unit II	16.63	2		
C0014G-2H-7 W, 90.0--92.0 cm	14-Unit II	18.56	2		

C0014G-3H-1 W, 8.0--10.0 cm	14-Unit II	18.78	2	illite, quartz, and Mg chlorite.	
C0014G-3H-7 W, 40.0--42.0 cm	14-Unit II	24.87	2		
C0014G-3H-9 W, 83.0--85.0 cm	14-Unit II	27.49	2		
C0014G-3H-CC W, 53.0--55.0 cm	14-Unit II	28.74	2		
C0014B-4H-5 W, 20.0--22.0 cm	14-Unit II	30.31	2		
C0014G-4H-6 W, 30.0--32.0 cm	14-Unit III	31.72	2		
C0014G-4H-7 W, 60.0--62.0 cm	14-Unit III	33.03	2		
C0014B-4H-7 W, 135.0--137.0 cm	14-Unit III	33.28	2	Silicified volcanic sediments (either matrix silicified or clasts and matrix silicifed), hydrothermally altered mud, mud, and sand with detrital hydrothermal component.	Hydrothermally altered sediments
C0014B-4H-9 W, 35.0--37.0 cm	14-Unit III	35.10	2		
C0014B-5H-3 W, 73.0--75.0 cm	14-Unit III	36.26	2		
C0014B-5H-4 W, 37.0--39.0 cm	14-Unit III	36.86	2		
C0014B-5H-5 W, 70.0--72.0 cm	14-Unit III	38.59	2		
C0014B-5H-12 W, 14.0--16.0 cm	14-Unit III	40.73	2		
C0014G-6H-6 W, 18.0--20.0 cm	14-Unit IV	51.55	2		
C0014G-9X-CC W, 30.0--32.0 cm	14-Unit IV	57.19	2		
C0014G-12H-2 W, 20.0--22.0 cm	14-Unit IV	64.53	2	Silicified volcanic sediments, hydrothermally altered mud as well as other volcaniclastic sedimentary rock	Hydrothermally altered sediments
C0014G-14T-2 W, 48.0--50.0 cm	14-Unit IV	72.16	2		
C0014G-18T-CC W, 7.0--9.0 cm	14-Unit IV	88.10	2		
C0014G-24T-3 W, 53.0--55.0 cm	14-Unit IV	111.23	2		
C0014G-30X-1 W, 5.0--7.0 cm	14-Unit IV	127.25	2		
C0017A-1H-1 W, 1.5--3.5 cm	17-Unit I	0.02	2		
C0017A-1H-1 W, 40.0--42.0 cm	17-Unit I	0.40	2		
C0017A-1H-2 W, 110.0--112.0 cm	17-Unit I	2.50	2		
C0017A-1H-4 W, 15.0--17.0 cm	17-Unit I	4.37	2	Hemipelagic mud is the dominant sediment type which is primarily composed of hemipelagic homogeneous silty clay or clayey silt, with widely distributed foraminifers and occasional lenticular pumiceous sand patches, gravels, and mud clasts.	Terrigenous and biological sediments
C0017A-1H-6 W, 30.0--32.0 cm	17-Unit I	7.34	2		
C0017B-1H-1 W, 80.0--82.0 cm	17-Unit I	9.60	2		
C0017B-1H-2 W, 110.0--112.0 cm	17-Unit I	11.31	2		
C0017B-1H-5 W, 30.0--32.0 cm	17-Unit I	14.74	2		
C0017B-1H-7 W, 30.0--32.0 cm	17-Unit I	17.57	2		
C0017C-1H-3 W, 100.0--102.0 cm	17-Unit I	22.12	2		
C0017C-1H-5 W, 30.0--32.0 cm	17-Unit I	24.24	2		
C0017C-2H-1 W, 24.0--26.0 cm	17-Unit II	28.04	2	Pumiceous gravel and lithoclast-rich horizons sediment type consists of poorly sorted pumiceous sediments dominated by coarse-grained angular woody pumiceous gravels.	Volcanic materials
C0017C-2H-CC W, 10.0--12.0 cm	17-Unit II	35.96	2		
C0017D-1H-4 W, 79.0--81.0 cm	17-Unit II	65.02	2		
C0017D-2H-3 W, 45.0--47.0 cm	17-Unit II	72.48	2		
C0017D-2H-6 W, 55.0--57.0 cm	17-Unit II	76.80	2		
C0017D-7H-2 W, 40.0--42.0 cm	17-Unit III	105.51	2		
C0017D-7H-5 W, 40.0--42.0 cm	17-Unit III	109.74	2	Hemipelagic mud and Pumiceous gravel. The components in this unit is likely the type between Unit I and Unit II.	Terrigenous and biological sediments
C0017D-9X-3 W, 40.0--42.0 cm	17-Unit III	123.53	2		
C0017D-9X-8 W, 27.0--29.0 cm	17-Unit III	130.38	2		
C0017D-10X-CC W, 24.0--26.0 cm	17-Unit III	136.96	2		

C0017D-11X-1 W, 50.0--52.0 cm	17-Unit III	140.70	2		
C0017D-11X-3 W, 29.0--31.0 cm	17-Unit III	143.30	2		
C0017D-11X-CC W, 1.0--3.0 cm	17-Unit III	144.35	2		
C0017D-11X-CC W, 36.0--38.0 cm	17-Unit III	144.70	2		
C0015B-1H-1 W, 12.0--14.0 cm	15-Unit I	0.12	2	Coarse pumiceous gravel and grit, siliciclastic sand, hemipelagic mud, bioclastic gravel, and foraminiferal sediment.	Terrigenous and biological sediments
C0015B-1H-2 W, 100.0--102.0 cm	15-Unit I	2.38	2		
C0015B-1H-4 W, 47.0--49.0 cm	15-Unit I	4.67	2		
C0015B-1H-4 W, 133.0--135.0 cm	15-Unit II	6.18	2	Pumiceous grit grading to gravel at base, Clast-supported coarse-grained angular pumice gravel.	Volcanic materials
C0015B-1H-5 W, 29.0--31.0 cm	15-Unit II	8.76	2		
C0016B01L0115-16	16-Unit I	0.15	2	Hard black clastic-textured massive sulfide	Hydrothermally altered sediments
C0016B01Lcc4-6	16-Unit II	~ 7	2	Hard gray strongly silicified volcanic rock, coarsely disseminated Sulfide.	Hydrothermally altered sediments
C0016B02Lcc3-4	16-Anhydrite	~ 12	2	Snow white coarsely crystalline anhydrite aggregate	Hydrothermally altered sediments
North Okinawa Trough Sufaces sediments	Background	0	2	Hemipelagic and biogenic sediment.	Terrigenous and biological sediments
North Okinawa Trough Sufaces rock	NOT-Volcanic	0		Volcanic rock	Volcanic materials

Table 2 Average of REEs parameters and Sr, Nd contents and isotopic compositions.

Sites	ΣREE (ppm)		δEu		$(La/Yb)_N$		Sr (ppm)	$^{87}Sr/^{86}Sr$	Nd (ppm)	εNd
	Residue	Leachate	Residue	Leachate	Residue	Leachate	Residue	Residue	Residue	Residue
Background	75.8	36.3	0.7	36.3	8.7	9.6	69.2	0.71690	13.4	-10.5
C0013-Unit I	161.3	9.9	0.6	9.9	4.2	129.2	2170.6	0.70877	26.1	4.0
C0013-Unit II	112.0	2.7	0.7	2.7	3.4	6.0	727.4	0.70881	26.5	6.0
C0013-Unit III	215.3	30.1	0.4	30.1	2.2	11.9	18.5	0.70897	39.0	5.9
C0013-Unit IV	129.6	6.6	0.3	6.6	2.9	7.9	1.2	0.70896	25.3	7.3
C0014-Unit I	97.8	47.7	0.6	47.7	7.1	8.5	55.8	0.71870	14.5	-8.1
C0014-Unit II	150.8	38.9	0.5	38.9	4.9	16.7	69.9	0.70913	25.1	0.1
C0014-Unit III	210.2	41.5	0.5	41.5	2.1	83.1	1.0	n.a.	32.3	5.1
C0014-Unit IV	172.7	26.6	0.5	26.6	1.9	37.9	2.8	0.70954	31.3	6.0
C0017-Unit I	90.6	44.8	0.6	44.8	8.7	8.4	105.2	0.72093	21.9	-10.9
C0017-Unit II	126.5	28.5	0.5	28.5	5.4	5.1	94.3	0.72277	21.0	-10.5
C0017-Unit III	104.4	56.4	0.7	56.4	7.5	9.9	100.5	0.72366	20.0	-12.1
C0015-Unit I	119.2	24.0	0.5	24.0	6.4	7.3	67.2	n.a.	28.8	n.a.
C0015-Unit II	140.8	28.0	0.5	28.0	2.3	2.0	7.9	n.a.	36.4	n.a.
C0016-Unit I	2.7	0.7	0.8	0.7	0.9	9.2	1.6	n.a.	0.6	3.8
C0016-Unit II	44.2	4.0	0.5	4.0	2.6	32.8	1.6	n.a.	7.5	6.3
C0016-anhydrite	2.1	2.1	0.7	2.1	9.2	9.6	1148.8	0.70881	0.6	-2.2
NOT-rock	16.1	58.0	2.3	58.0	1.6	3.8	132.0	0.70486	2.6	1.2

n.a.: not analyzed.

$\varepsilon Nd = (^{143}Nd/^{144}Nd)_{Sample}/(^{143}Nd/^{144}Nd)_{Standard}-1]\times10^4$, where "Standard" is chondritic uniform reservoir value (Bouvier et al., 2008).

Figure captions:

Figure 1

Maps showing the (a) study area and (b) locations of IODP Expedition 331 drill sites in the Okinawa Trough. (c) The inferred dispersal pattern of hydrothermal fluid in the study area. (Modified from Expedition 331 Scientists Preliminary Report, 2011).

Figure 2

Mineralogical composition of hydrothermal sediments, volcanic rocks, and background surface sediments.

Figure 3

Major and minor elements in the residue and leachate fractions normalized to the average composition of upper continental crust (UCC). Elemental compatibility increases from left to right.

Figure 4

Chondrite-normalized (Boynton, 1984) rare earth element (REE) patterns for hydrothermal sediments, volcanic rocks, and background surface sediments.

Figure 5

Sr-Nd elemental and isotopic compositions in residue fraction. OT-pumice and andesite/basalt data from Ryuichi Shinjo et al (1999, 2000); Seawater data from Piepgras et al. (1979).

Figure 6

High-field-strength elements concentrations and ratios in hydrothermal sediments, volcanic rocks, terrigenous sediments and reference data (Shinjo, 1999; Shinjo et al., 1999; 2000).

Figure 7

Chondrite-normalized (Boynton, 1984) REE patterns of volcanic rocks (Shinjo, 1999; Shinjo et al., 1999; 2000) and C0015-Unit II normalized REE patterns of chlorite-rich sediment.

Figure 8

Chondrite-normalized (Boynton, 1984) REEs patterns of anhydrite-rich sediments at site C0013 and C0016 and hydrothermal fluid from references. TAG-black and TAG- white hydrothermal fluid data from Mitra et al. (1994); OT-fluid data from Hongo et al. (2007); seawater data from Alibo and Nozaki (1999).

Figure 9

Schematic diagrams of hydrothermal system in the Iheya North Knoll, Okinawa Trough. (a) Geological settings of the OT. (b) Stratigraphy of IODP Expedition 331 drill cores and inferred fluid flow (Modified from Expedition 331 Scientists, 2011; Miyoshi et al., 2015).

Fig. 1 Shao et al., 2016

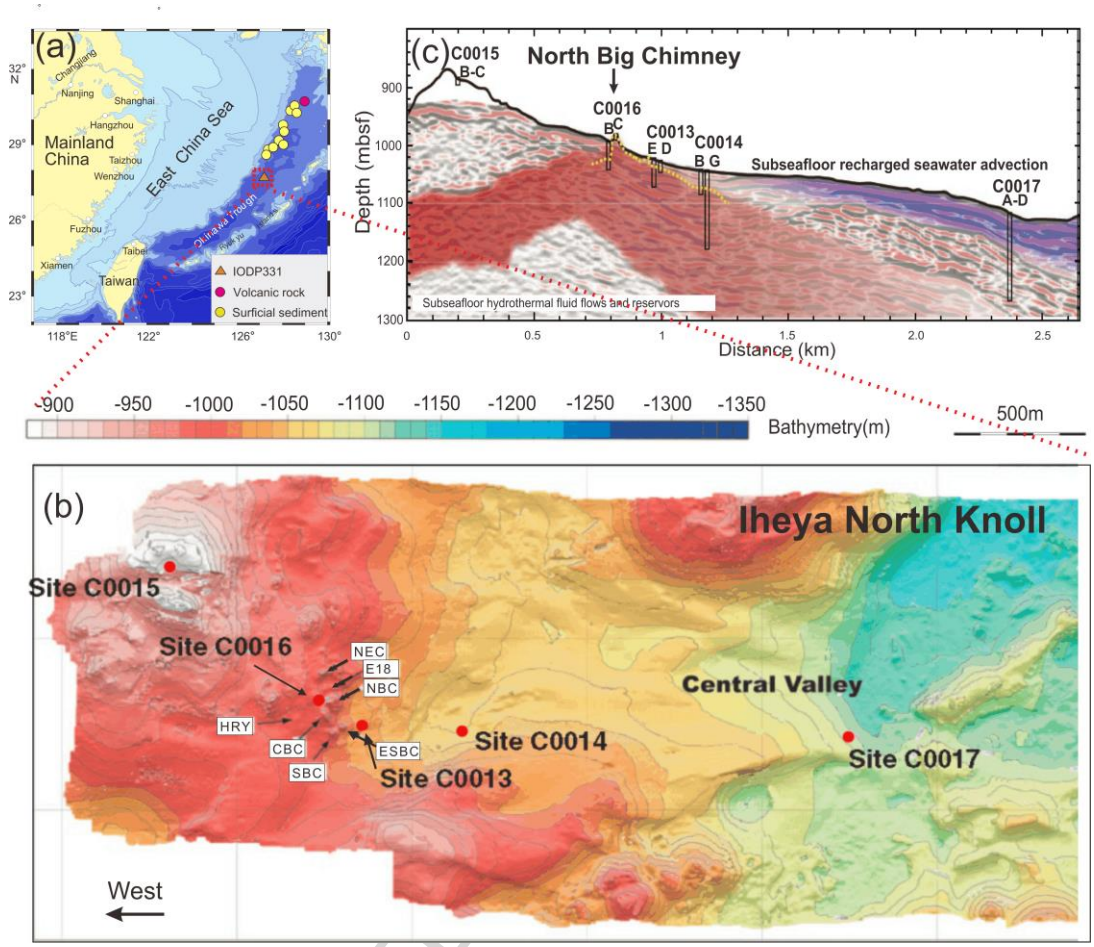

Fig. 2 Shao et al., 2016

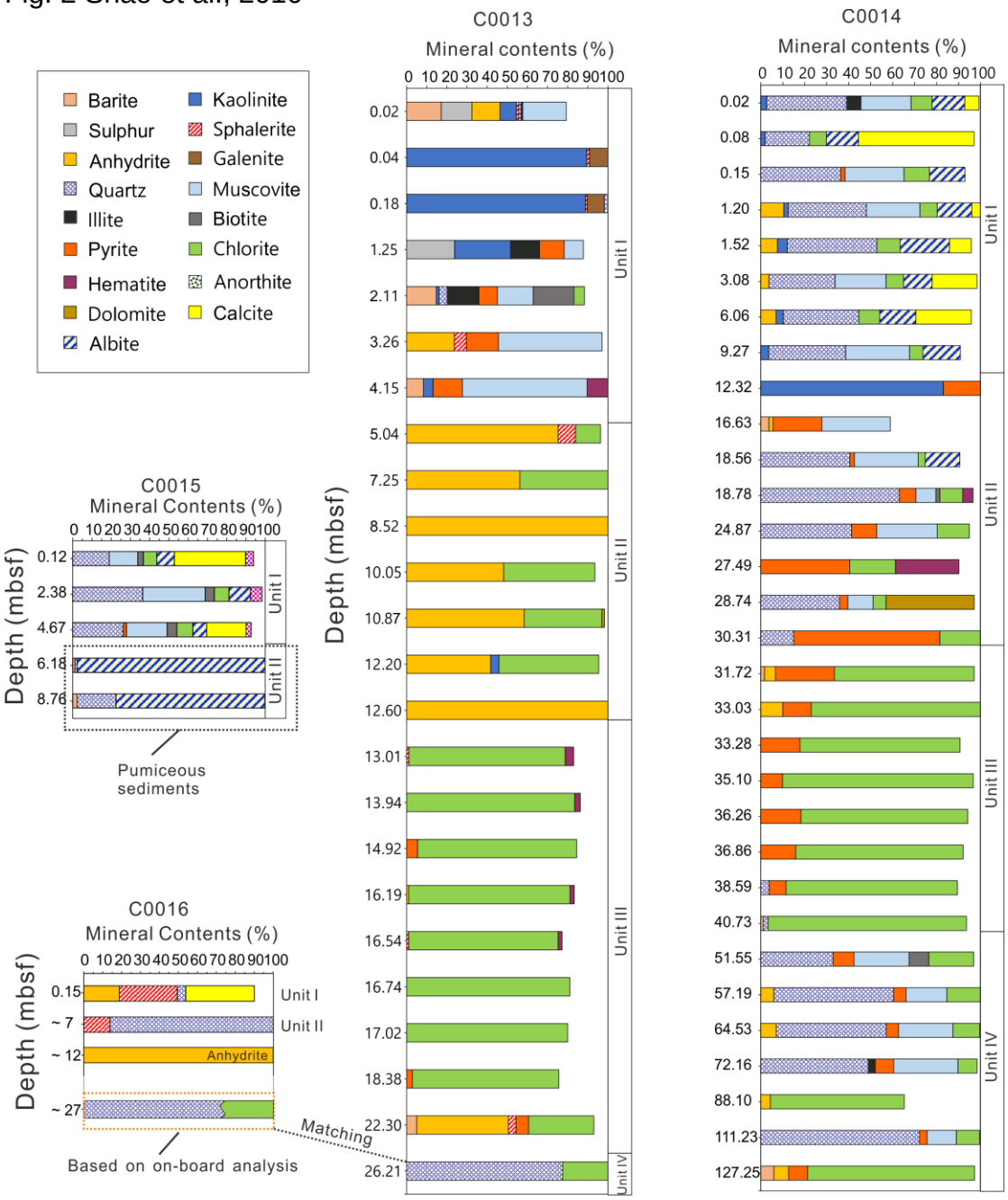

Fig. 2 Continued

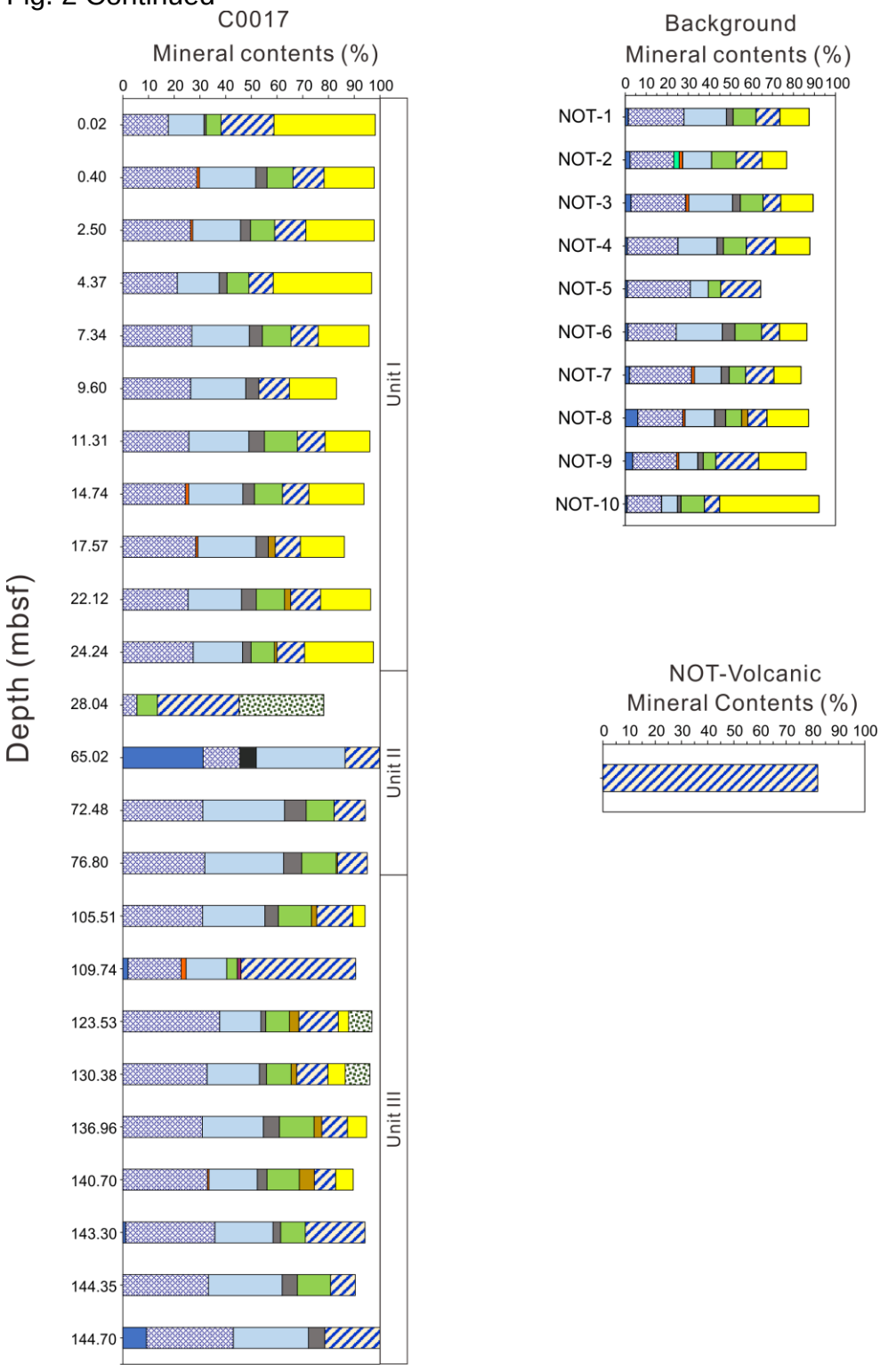

Fig. 3 Shao et al., 2016

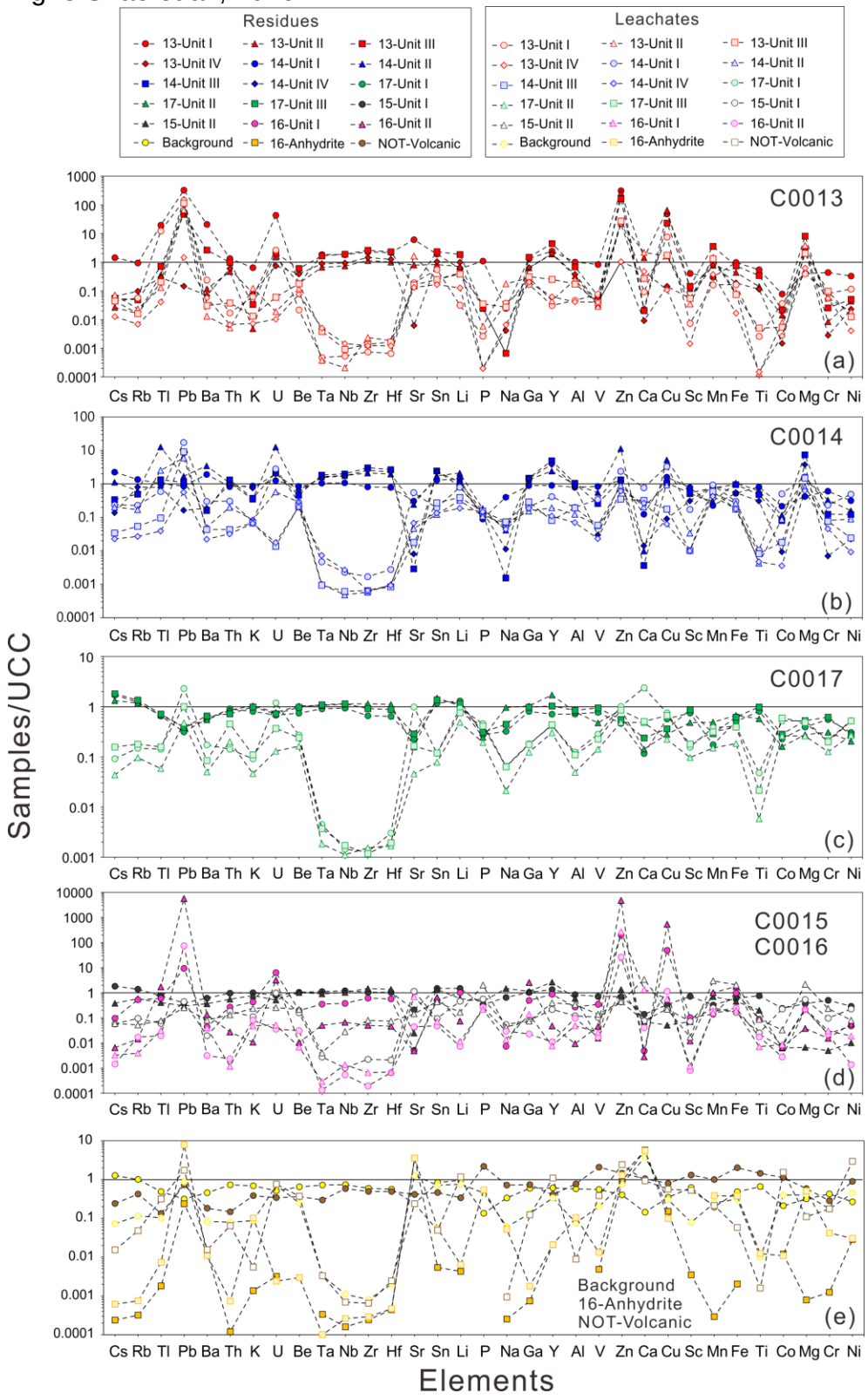

Fig. 4 Shao et al., 2016

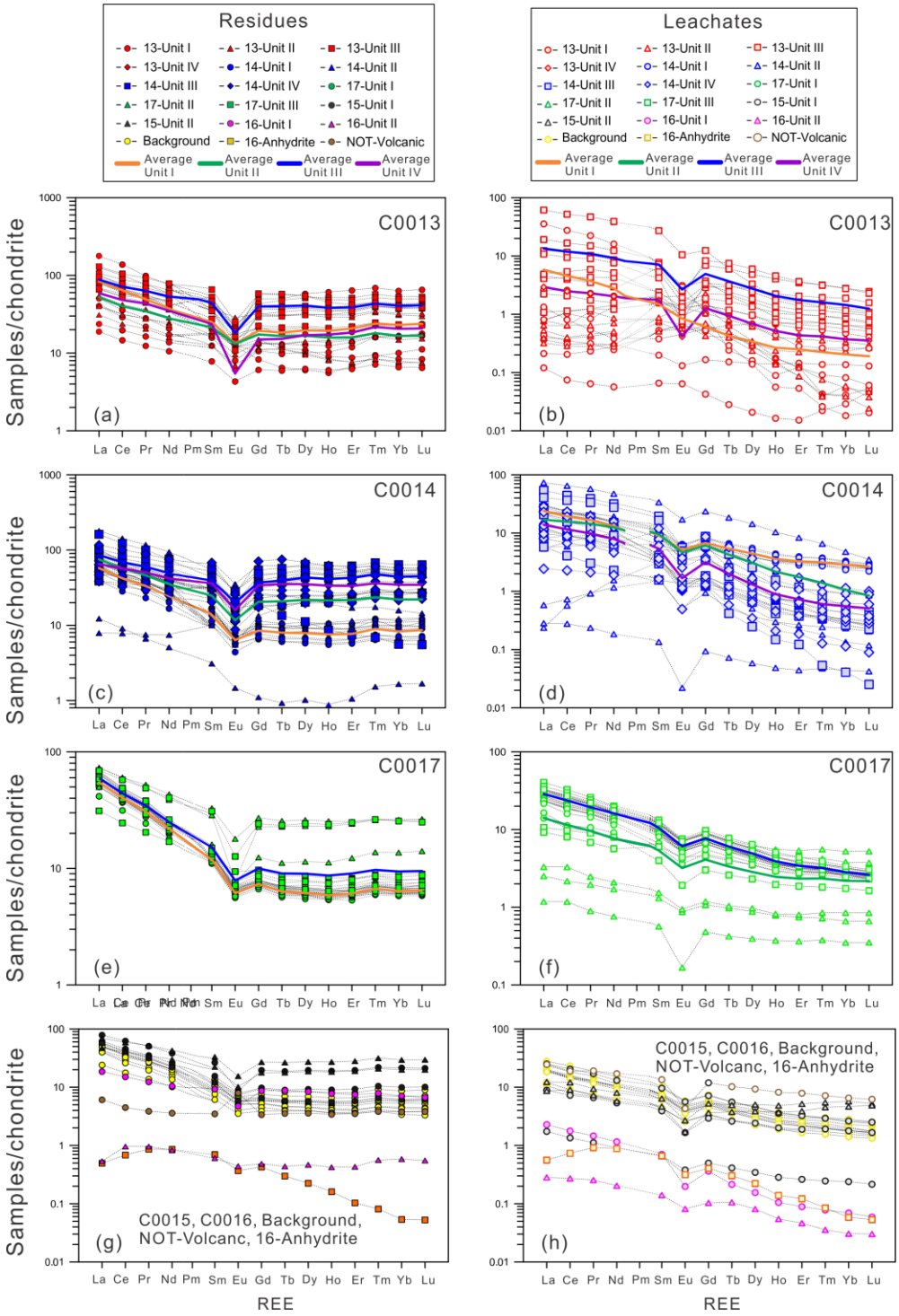

Fig. 5 Shao et al., 2016

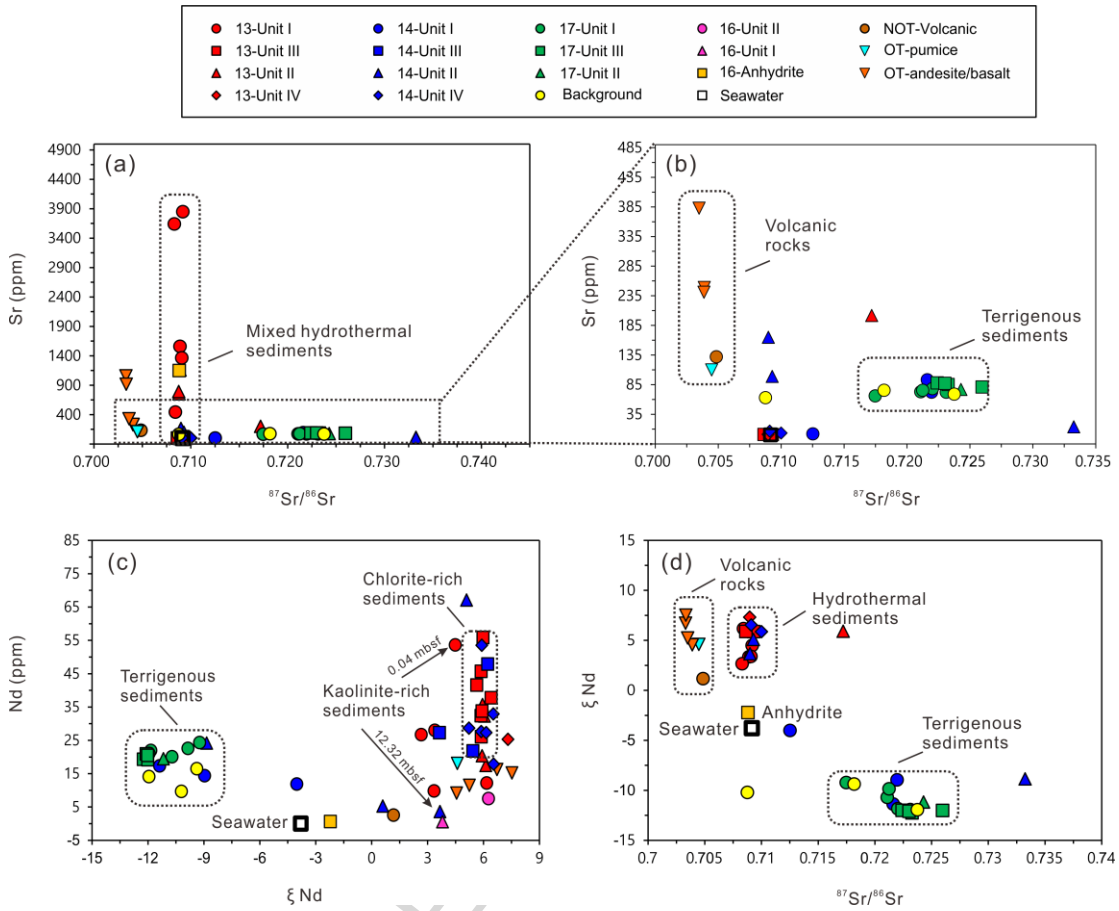

Fig. 6 Shao et al., 2016

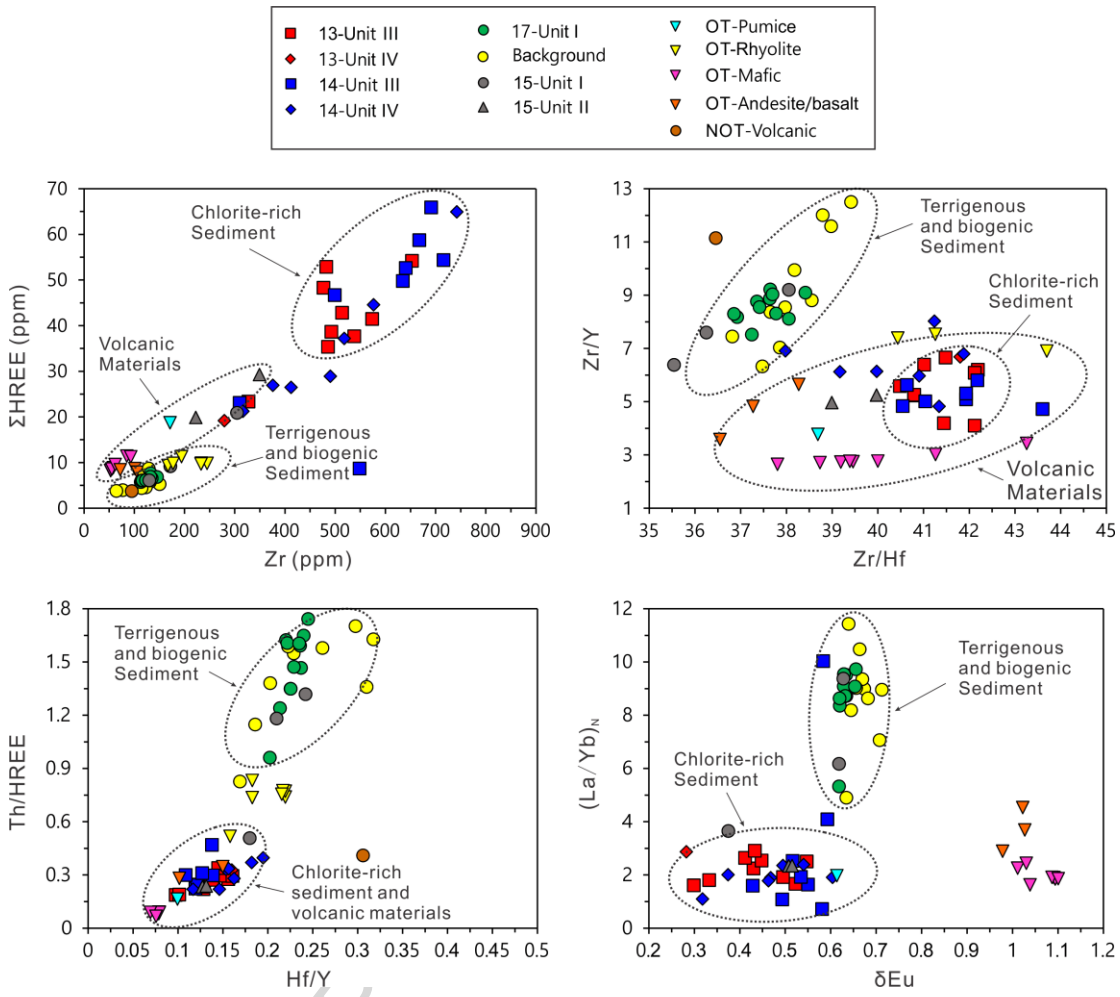

Fig. 7 Shao et al., 2016

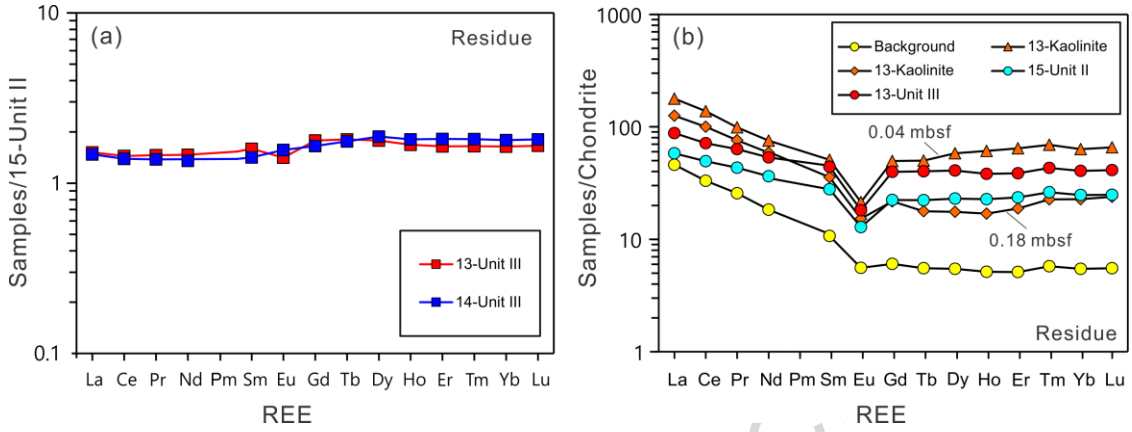

Fig. 8 Shao et al., 2016

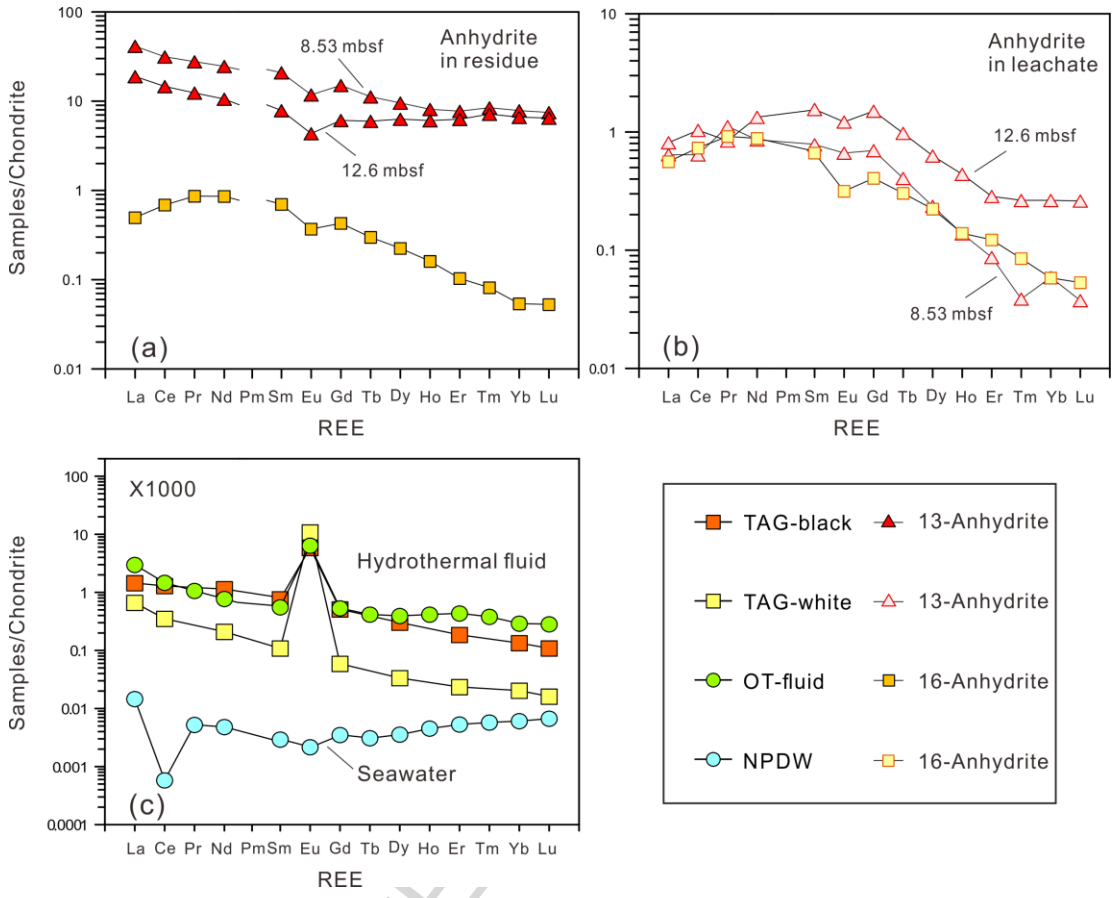

Fig. 9 Shao et al., 2016